Atmos. Chem. Phys. Discuss., 7, 15739–15779, 2007
www.atmos-chem-phys-discuss.net/7/15739/2007/

Atmospheric Chemistry and Physics Discussions

20-year LiDAR observations of stratospheric sudden warming over a mid-latitude site, Observatoire de Haute Provence (OHP; 44° N, 6° E): case study and statistical characteristics

D. V. Charyulu[1,2], V. Sivakumar[3], H. Bencherif[1], G. Kirgis[1,4], A. Hauchecorne[4], P. Keckhut[4], and D. Narayana Rao[2]

[1]Laboratoire de l'Atmosphère et des Cyclones, UMR 8105 CNRS/Université/Météo-France, Université de LaRéunion, Messag 9 BP 1751, Saint Denis, Réunion Island, France
[2]National Atmosphere Research Laboratory, Tirupati, Andhra-Pradesh, India
[3]National Laser Centre, Council for Scientific and Industrial Research (CSIR), P.O. Box 395, Pretoria 0001, South Africa
[4]Service d'Aéronomie, IPSL, UMR CNRS, Paris, France

Received: 28 June 2007 – Accepted: 25 September 2007 – Published: 12 November 2007

Correspondence to: D. V. Charyulu (vidya@univ-reunion.fr)

Abstract

The present study delineates the characteristics of Stratospheric Sudden Warming (SSW) events observed over the Observatoire de Haute Provence (OHP: 44° N, 6° E). The study uses 20 years of Rayleigh LiDAR temperature measurements for the period, 1982–2001, which corresponds to 2629 daily temperature profiles. Characteristics of warming events, such as type of warming (major and minor), magnitude of warming, height of occurrence and day period of occurrence are presented with emphasis on wave propagation and isentropic transport conditions. The major and minor warming events are classified with respect to temperature increase and reversal in the zonal wind direction in the polar region using reanalysis data from the National Centre for Environmental Prediction (NCEP). SSWs occur with a mean frequency of 2.15 events per winter season. The percentage of occurrence of major and minor warming events are found to be ∼23% and ∼77%, respectively. The observed major and minor SSW is associated with a descent of the stratopause layer by −6 to 6 km range. The heights of occurrences of major SSWs are distributed between 38 km and 54 km with magnitudes in the 12.2–35.7 K temperature range, while minor SSW occurrences appear in the 42–54 km range, closer to the usual stratopause layer (∼47 km) and with a slightly larger range of temperature magnitude (10.2–32.8 K). The observed major and minor events are examined in connection with Quasi-Biennial Oscillation (QBO) phases.

1 Introduction

The middle atmosphere (which mainly covers stratosphere and mesosphere) is the region of the atmosphere from approximately 12 km to 80 km altitude. Studies of dynamic, radiative and chemical processes in this region have expanded greatly in recent years owing to impacts by human activities on the stratospheric ozone layer and the coupling between stratospheric changes and surface climate (McIntyre, 1982; Andrews et al., 1985).

ACPD

7, 15739–15779, 2007

It is well known that there is a large interannual temperature variation in the Northern Hemisphere winter stratosphere. The greatest variation is observed due to Stratospheric Sudden Warming (hereafter, referred as SSW) (Scherhag 1952; Labitzke, 1977, 1981, 1982; Schoeberl, 1978; Quiroz, 1986; Andrews et al., 1985) and so far, evidence shows that the occurrence of SSW, may have a marked influence on polar stratospheric temperatures (e.g., Matsuno, 1971; Andrews et al., 1985), troposphere circulation (e.g., Quiroz, 1977; O'Neill and Taylor, 1979; Baldwin and Dunkerton, 1999) Northern Hemisphere annular mode (NAM) and on zonal flow in the Upper Troposphere-Lower Stratosphere (UT-LS) region (e.g., Limpasuvan et al., 2004). Historically, SSW has been viewed as a large-scale dynamical meteorological phenomenon in the stratosphere. Observational, theoretical and modeling studies on SSW have expanded greatly in recent years in attempts to understand the stratospheric circulation and relate it to dynamical-chemical changes with emphasis on stratosphere ozone content.

Briefly, during some winters, the zonal-mean configuration is dramatically disrupted with polar stratospheric temperatures increasing rapidly with time, leading to a poleward increase of zonal-mean temperatures and on occasion, a reversal of zonal-mean winds to an easterly direction exists. Such an event is defined as Stratospheric Sudden Warming (SSW) (Andrews et al., 1985). It is a large-scale dynamic event with a QBO signature of occurrence (Baldwin et al., 2001) which could increase the temperatures near the pole by ~40–60 K in one week. Major warmings may not occur every winter, but occur mostly in every alternative winter. Minor warmings do occur more frequently in every winter (e.g. Andrews et al., 1985; Dunkerton and Baldwin, 1991). Major warming occurs mostly during mid-winter in Northern Hemisphere, resulting in the strongest perturbations in zonal-mean temperature and zonal-mean wind reversal (westerly to easterly) (Lorenz, 1967; Dunkerton and Baldwin, 1991).

In addition, a SSW may either cause a polar vortex displacement from the pole or may split the vortex into two parts (often referred as SSW generated by wavenumber 1 and wavenumber 2). Some major warmings exhibit a hybrid character with the split

ACPD
7, 15739–15779, 2007

EGU

polar vortex being displaced asymmetrically from the pole. On the other hand, minor warmings occur every winter with weaker perturbations in zonal-mean temperature and no reversal of the zonal-mean wind. Furthermore, they do not lead to polar vortex displacement or vortex splitting. Final warmings occur at the end of the winter and they mark the transition between winter westerly winds and summer easterly winds which leads to polar vortex breakdown. Canadian warmings may occur in early winter (mid-November to early December) showing abrupt temperature increases similar to the major warmings. During Canadian warmings, the warm Aleutian High advects eastward with in a few days from its usual position over the dateline towards 90° W line of longitude over Canada. In this case, the polar vortex does not breakdown but distorts strongly and displaces from the pole (Andrews et al., 1985; Donfrancesco et al., 1996; Marenco et al., 1997; O'Neill, 2003).

The investigation of stratospheric warming has been greatly advanced in recent years, using conventional data retrieved from radiosondes, rocketsondes, falling spheres, ground based LiDAR and satellite data. In order to measure continuous short term changes in temperature over long periods of time and over a particular place, ground based LiDAR techniques are advantageous due to its good range and superior temporal and altitude resolution. Other techniques like satellites, which offer the temperature structure over the globe with good temporal coverage, are unable to provide the high altitude resolution. Rocketsondes and falling spheres offer relatively poor vertical resolution and accuracy due to uncertain radiative and aerodynamic heating corrections. Another advantage in LiDAR monitoring is that it is economical in comparison with other techniques. In fact, LiDAR may be operated continuously at different places during specific campaigns or routinely for long-term survey with limited financial and manpower resources (Labitzke and van Loon, 1999).

So far, many observational studies were carried out in order to characterize SSW events using temperature measurements from LiDAR, satellite and rockets over the Northern and Southern Hemispheres. Such warming events, based on temperature and zonal wind fields, have been individually classified as major, minor or Canadian

ACPD
7, 15739–15779, 2007

warmings. Most of these events are documented in the literature as case studies but few statistical results are available (e.g. Appu, 1984; Dunkerton and Delisi, 1986; Delisi and Dunkerton, 1988; Dunkerton et al., 1988).

The first SSW observation was reported by Scherhag in 1952, using radiosonde measurements over Berlin. Later, Schoeberl (1978) provided a review on the theory and observations of stratospheric warming using results reported from different places. The results suggested that the warming is confined to the Northern Hemisphere, especially during winter over polar region (Andrews et al., 1985). Similarly, there is also evidence of SSW occurrences in the Southern Hemisphere (e.g. Baldwin et al., 2003). The cause of SSWs is mainly attributed to planetary wave breaking (Hauchecorne and Chanin, 1983; Marenco et al., 1997) and gravity wave propagation (Whiteway and Carswell, 1994; Whiteway et al., 1997). There are many results reported as case studies for high latitude (Whiteway and Carswell, 1994; Donfrancesco et al., 1996; Whiteway et al., 1997; Duck et al., 1998; Walterscheid et al., 2000) and very rarely for mid- (Hauchecorne and Chanin, 1983) and low-latitudes (Sivakumar et al., 2004). The recent observation made by Sivakumar et al. (2004) recorded the first finding of a SSW over low latitudes and illustrated that the warming is due to an increase in planetary-wave activity. Their calculations on Eliassen-Palm (E-P) flux from ECMWF reanalysis, shows clear evidence of an equator-ward propagation of planetary waves consecutive to a major warming episode over polar region. The study evidenced that the SSW is not only focused towards high/mid latitudes, but that it can also extend to low latitudes depending on the strength of the warming. So far, most studies on SSW have been addressed at high latitude regions and for limited observational periods. Even then, there is no long database available to address such phenomenon for a extensive statistical study.

We use the 20 years of ground-based LiDAR data collected at the Observatoire de Haute Provence (OHP; 44° N, 6° E) from January 1982 to November 2001, to investigate SSW characteristics. OHP is a French observatory that acts as a primary NDACC (Network for the Detection of Atmosphere Composition Change) site. OHP

ACPD
7, 15739–15779, 2007

Rayleigh LiDAR has been operating regularly since 1979, and serves as a long-term dataset in studying and understanding the mid-latitude middle atmosphere thermal structure and dynamics (e.g. Hauchecorne and Chanin, 1980, 1983; Randel et al., 2002; Hauchecorne et al., 2002).

The present paper is structured as follows: Sect. 2 gives details about the datasets and analyses tools used to examine SSW events. In Sect. 3, we discuss the OHP observed LiDAR temperature evolution and calculations of climatological and seasonal mean profiles. Section 4 presents a case study on the winter-1998/1999 and introduces the criteria involved to identify and classify SSW events over OHP. Results and discussions on observed statistical characteristics of SSWs such as dates of occurrence, duration of occurrences, magnitude of warm temperature, descent height of stratopause, occurrence of SSW according to the state of QBO and agreement of date of occurrence of SSWs with previous reports are presented in Sect. 5.

2 Data and analysis

2.1 Daily temperature profiles

2.1.1 LiDAR profiles

A LiDAR dataset refers to a night time temperature profile measured by a ground based Rayleigh LiDAR system located at the Observatoire de Haute Provence (OHP; 44° N; 6° E), south of France. Temperature profiles are retrieved from the back-scattered photons in each successive atmospheric layer. The back-scattered photons provide the vertical profile of relative atmospheric density. Assuming that the atmosphere is in hydrostatic equilibrium, a pressure profile can be computed by combining a reference atmospheric model and a measured density profile along the studied height range (typically 30–80 km) with a height resolution of 300 m (Hauchecorne and Chanin, 1980; Chanin and Hauchecorne, 1984). Adopting the perfect gas law and using the derived

ACPD
7, 15739–15779, 2007

density and pressure profiles, the temperature profile can be deduced by following the retrieval method developed by Hauchecorne and Chanin (1980).

A 20-year LiDAR dataset covering the period from 1 January 1982 to 6 November 2001 is used to examine the middle atmosphere thermal structures to detect SSW events over OHP. The total number of observations correspond to 2629 and are distributed almost evenly in each month. The monthly distribution of LiDAR observations is presented in terms of a histogram in the Fig. 1. It illustrates an average number of observations of ∼225 profiles per month. In order to examine the seasonal characteristics of temperature over OHP, the 2629-daily LiDAR profiles are grouped into each three months in the following manner;

- 749 records during winter (December–January–February: DJF),
- 580 records during spring (March–April–May: MAM),
- 639 records during summer (June–July–August: JJA), and
- 661 records during autumn (September–October–November: SON).

Based on earlier reported results, SSW events occur only during winter and nearby periods. This leads us to enlarge the winter period by including the early and late winter LiDAR records: the enlarged winter is from November to March and it is made of 1233 temperature profiles (i.e. ∼47% of the complete LiDAR datasets).

Besides the above LiDAR observations, additional datasets are required to classify and interpret the noticed SSW events. The following sub-sections give a brief description of UARS/HALOE, NCEP, ECMWF-ERA40 datasets and of the high-resolution MIMOSA model.

2.1.2 UARS/HALOE profiles

Halogen Occultation Experiment (HALOE) is on board the Upper Atmosphere Research Satellite (UARS) launched on 12 September 1991. It uses solar occultation

ACPD
7, 15739–15779, 2007

method to measure vertical profiles of Ozone (O_3), Hydrogen Chloride (HCl), Hydrogen Fluoride (HF), Methane (CH_4), Water Vapor (H_2O), Nitric Oxide (NO), Nitrogen Dioxide (NO_2), Temperature and Aerosol Extinction at 4 infrared wavelengths. It uses the atmospheric transmission measurements in the 2.8-μm CO_2 and for the retrieval of temperature profiles. The temperature data obtained after the removal of aerosol contamination (Net-ASCII, Version 19). Further detailed descriptions of HALOE satellite data are available on the web (http://haloedata.larc.nasa.gov/home/index.php). Information about validation and accuracy of HALOE data can be found in published papers: Russel et al. (1993); Hervig et al. (1996); Sivakumar et al. (2003, 2004).

In the present study, quasi-simultaneous measurements (same date as LiDAR measurements) of UARS/HALOE (sunrise and sunset) overpasses over OHP (44° N, 6° E) site, within ±5° in latitude and ±10° in longitude ranges from winter 1991/1992 to winter 2001/2002 are examined.

3 Meteorological data

3.1 NCEP data

The National Center for Environmental Prediction (NCEP) provides daily meteorological data on a 2.5°×2.5° horizontal grid for 17 pressure levels: between 1000- and 10-hPa (Kalnay et al., 1996). Earlier reports suggest that the North Pole NCEP temperatures in winter, particularly in February and March, during 1979–2001, are in very good agreement with FU-Berlin data and ECMWF-ERA40 reanalysis datasets (Labitzke and Kunze, 2005). NCEP/NCAR reanalysis data is archived on the NOAA Climate Diagnostics Center web page (http://www.cdc.noaa.gov/). In the present study, we use a NCEP zonal mean temperature at 80° N and zonal mean wind at 60° N at the 50-, 30-, and 10-hPa pressure levels to examine temperature and wind conditions over the pole.

3.1.1 ECMWF-ERA40 re-analysis data

Information about prevailing meteorological and dynamical conditions in the northern stratosphere is addressed using ERA40 re-analyses. The latter is archived on the ECMWF (European Centre for Medium-Range Weather Forecasts) website, http://www.ecmwf.int/research/era/. Indeed, ECMWF-ERA40 horizontal winds and temperature fields are extracted on a 2.5°×2.5° grid from 1000- to 1-hPa pressure levels. The extracted data is used in the present study to derive the Ertel's Potential Vorticity (EPV) and Eliassen-Palm (E-P) flux.

4 Dynamics/transport analysis tools

4.1 EPV contour advection by MIMOSA model

MIMOSA (Modélisation Isentrope du transport Mésoéchelle de l'Ozone Stratosphérique par Advection) is a high-resolution advection contour model of the Ertel's Potential Vorticity (EPV). It was developed at the Service d'Aéronomie, a French CNRS research unit, by Hauchecorne et al. (2002). The model can be used both to reproduce global atmosphere dynamical events and small-scale events and especially to interpret the events such as ozone or aerosol laminae (Bencherif et al., 2003; Morel et al., 2005; Semane et al., 2006). The model starts from the ECMWF PV field interpolated on the MIMOSA orthogonal grid. The PV of each grid-point is advected using ECMWF winds. The model runs on an isentropic surface and two domains centred at the North and South poles with a resolution of 3 points grid per degree. The fields produced for each hemisphere are then linked together within a latitude band of 5° width, centred over the equator. A full description of the MIMOSA model is given in Hauchecorne et al. (2002).

In the present study, the MIMOSA model is run in order to construct Advected Potential Vorticity (APV) maps on stratospheric isentropic levels.

ACPD
7, 15739–15779, 2007

4.2 Eliassen-Palm flux

In order to gain insights into the dynamical processes occurring during SSW events and in particular to study the planetary wave drive and breaking, the Eliassen-Palm (E-P) flux vector (F) and its divergence (∇F) are used. It is defined by the following equations (Andrews et al., 1987):

$$F = \left\{f_{(\phi)}, F_{(z)}\right\} = \left\{-\rho_0 a \cos\phi \left(\overline{v'u'}\right), f\rho_0 a \cos\phi \left(\frac{\overline{v'\theta'}}{\overline{\theta'}}\right)\right\} \text{ and}$$

$$\nabla.F = \frac{1}{a\cos\phi}\left(F_\phi \cos\phi\right)_\phi + \left(F_{(z)}\right)_z \quad (1)$$

The over-bars denote zonal means and primes denote the deviations with their respective means. The other symbols have usual meanings. Further explanations may be found in Andrews et al. (1987).

During winter, Planetary Waves (PW) generally propagates from the troposphere to the stratosphere and towards the equator (Eliassen and Palm, 1961; Kanzawa et al., 1984). These waves highly disturb the middle atmosphere temperature and act as one of the generative mechanism for the occurrence of SSW. The orientation of E-P flux vectors indicates the direction of Planetary Wave propagation (Dunkerton and Delisi, 1986; Delisi and Dunkerton, 1988) and the convergence of the E-P vectors ($\nabla.F < 0$) indicate the Planetary Wave (PW) breaking.

5 Seasonal variability of temperature

This section aims to illustrate the general temperature behavior and the seasonal mean temperature profiles as derived from OHP LiDAR observations. The time evolution, recorded by LiDAR, of temperature, for the 30–70 km altitude range is depicted in Fig. 2. The blank spaces in the figure correspond to the actual data gap.

ACPD
7, 15739–15779, 2007

EGU

In order to underline the climatological thermal structure and corresponding variability in terms of seasonal variation of mean temperatures and respective standard deviations, the winter, spring, summer and autumn mean temperature profiles are obtained as follows; daily temperature profiles of the months of December–January–February (winter), March–April–May (spring), June–July–August (summer) and September–October–November (autumn) data are grouped irrespective of the year (from 1982 to 2001) and averaged to obtain one value per day and per kilometer. Similarly, enlarged winter/summer mean profiles are calculated by taking into account early and late winter/summer months (i.e. enlarged winter: November to March; enlarged summer: May to September). The obtained seasonal profiles are presented in the Fig. 3. The overall temperature profile, obtained by averaging the 20-year dataset irrespective of month and year, is superimposed (with start symbols). It shows a maximum temperature of ~264.5 K and a stratopause height at ~47 km. The observed stratosphere – lower mesosphere region is warmer during summer and cooler during winter. The summer stratopause is found at ~47.5 km with a maximum temperature of ~268 K. The winter stratopause is found to occur at ~45.5 km with a maximum temperature of ~262 K, which is used as a reference value in the present study to calculate the descent of stratopause and the magnitude of the warm temperature respectively. At the stratopause height, the minimum temperatures are observed in the beginning of November and the maximum temperatures are observed in May–June period (figure not shown). This is in agreement with previous climatological studies for OHP site (Hauchecorne et al., 1991; Hauchecorne and Chanin, 1983; Leblanc et al., 1998; Sivakumar et al., 2006).

From seasonal temperature profiles (Fig. 3), one can see that spring and summer profiles exhibit a similar behavior at the stratopause region in terms of height (stratopause at ~47.5 km) and temperature (~268 K). The maximum descent of stratopause is obtained during winter (~45.5 km). Note that by January the stratopause is found (figure not shown) at its lowest height (~45 km). The enlarged winter (NDJFM) and summer (MJJAS) profiles and the respective standard deviations are presented in

ACPD
7, 15739–15779, 2007

Fig. 4 (a and b). For ease of comparison, the figure is superimposed by the 20-year over-all temperature profile. As expected, it is evidenced from the figure that winter deviations (±12 K) are approximately four times larger than summer deviations (±3 K) at usual stratopause level. This is consistent with wave disturbances increasing in the winter hemisphere. In fact, the winter stratosphere is disrupted mainly by gravity and planetary wave activity. These waves are generated mainly in the troposphere and in winter, they propagate with the westerly winds through the middle atmosphere.

6 SSW: A case study

6.1 SSW detection and classification criteria

A stratospheric sudden warming event is classified as major, minor, Canadian or final warming (e.g., O'Neill, 2003). The final warming characteristics are similar to the major warming, except that it occurs mostly during the end of winter. Both the major and final warmings lead to a breakdown of the cyclonic polar vortex. Therefore, in the present study, we classify the final warming as a major warming. Further, a warming is said to be Canadian when it occurs over Aleutian High region (Canada), (e.g., Labitzke and van Loon, 1999; O'Neill, 2003). Here, we classified the observed warming events into either minor or major warmings. In this regard, daily profiles are compared to the extended winter (NDJFM) mean profile.

When a temperature profile is 10-K (or 2σ) warmer than the enlarged-winter mean profile, we examine the zonal parameters in the polar stratosphere (using NCEP data at the 10-hPa pressure level), i.e., temperature and wind components at 80° N and 60° N respectively. A warming event is detected if the temperature evolution over polar region illustrates a significant increase. Further, if the warming is coincident with a zonal wind reversal (i.e., it becomes easterly), the warming is classified as a major one; otherwise it is classified as a minor.

ACPD
7, 15739–15779, 2007

6.1.1 Case study

As a case study, we investigate the SSW events observed during winter (NDJFM) 1998/1999. The corresponding temporal evolution of lidar temperature profiles from 1 November 1998 to 31 March 1999 is presented in the Fig. 5. During the above-said period, there are occurrences of missing LiDAR data (blank spaces). The figure illustrates the warm temperature in the stratopause height region. It is observed that on a few occasions, the values are greater than 280 K. However, on Fig. 4a, one can see that the stratopause is as high as ∼47 km with a maximum temperature of ∼261 K.

Taking into account temperature differences between LiDAR daily profiles and the enlarged-winter profile (sometimes more than +20 K), one can underline that the observed stratosphere was under several and successive warmings during winter 1998/1999. For illustration purposes, daily profiles corresponding to two successive warming episodes (i.e., 4–8 and 16–19 December) are shown in Fig. 7 (a and b), together with the over-all and the enlarged-winter profiles. Those two warming episodes do not exhibit similar temperature characteristics. However, it is observed that both of them are consistent with the quasi-simultaneous HALOE temperature profiles (derived from UARS/HALOE overpasses nearby OHP location at ±5° in latitude and ±10° in longitude).

By combining LiDAR observations and NCEP reanalysis, this case study section aims to focus on detection of warming events that occurred during the 1998/1999 winter over a mid-latitude site (OHP), following the detection criteria explained above.

- Early-December, Early January and Mid January > minor warming occasion and
- Mid-December > major warming occasion,

The noticed SSW temperature profiles for the above four occasions correspond during 4 to 8 December 1998, 16 to 19 December 1998, 5 to 9 January 1999 and 13 to 14 January 1999. To compare and classify the above said four SSW events into Major or Minor warmings, the NCEP data of zonal-mean temperature at 80° N and zonal mean

ACPD
7, 15739–15779, 2007

wind at 60° N at three different pressure levels (50, 30 and 10 hPa) are presented for the period from November 1998 to March 1999 in Fig. 6. The zonal mean temperature and wind at three different pressure levels follow each other. For classifying the events into a major/minor category, we have used only the temperature/wind information for the pressure levels at 10 hPa. Among the temperature profiles of the first SSW event from 4 to 8 December 1998, the warmest temperature profile is observed on 6 December 1998. The warm stratopause located at 46 km (see Fig. 7a) is in good agreement to compare the temperatures at 10 hPa (about 30 km) pressure level observed on the same day by NCEP (see Fig. 6). However, no zonal mean wind reversal is observed (in NCEP data) for the same day or few days before to the 6 December 1998. Therefore, the SSW event noticed on 6 December 1998 is classified as minor warming. Whereas, during the second SSW event from 16 to 19 December 1998, the maximum temperature is observed on 17 December 1998 and, is again, in good agreement for comparison with the NCEP observations. The peak in the NCEP temperature is noticed on the same day (see Fig. 6) and zonal mean wind reversal is also observed (in NCEP data) on the same occasion. Therefore, this SSW event, on 17 December 1998, is classified as major warming. Similarly, the third SSW event occasion from 5 to 9 January 1999, the warmest day temperature profile is observed on 7 January 1999, which is in agreement after comparing the peak temperature observed on the same day by NCEP at 10 hPa (Fig. 6). No zonal mean wind reversal is observed (in NCEP data) a few days before to the 7 January 1999, so, the SSW event noticed on 5 January 1999 is classified as minor warming. The fourth SSW event recorded warm temperatures observed on the 13 and 14 January 1999. The warmer day temperature profile observed on 14 January 1999 is in good agreement to compare the temperatures observed on the same day by NCEP (Fig. 6). In the same period, no zonal mean wind reversal is noticed in the NCEP data sets and therefore this event (14 January 1999) is classified as minor warming. The time gap in the occurrence between these four SSW events is 11 days, 20 days and 7 days. Warm temperature of 15.1 K, 28.7 K, 18.1 K and 14.4 K is noticed on the above four SSWs (6 December 1998 (minor), 17 December

ACPD
7, 15739–15779, 2007

EGU

1998 (major), 7 January 1999 (minor), and 14 January 1999 (minor)) respectively. Descent of stratopause occurred at ∼1 km, ∼6 km, ∼2 km and ∼3 km respectively. All of the four above mentioned SSWs have occurred when the QBO was in the west phase.

Among the above noticed four SSW events, we have chosen the first (6 December 1998 – Minor SSW) and second (17 December 1998 – Major SSW) events to illustrate the method of analysis. Figure 7a and b shows daily profiles of temperatures observed from 4 to 8 December 1998 and from 16 to 19 December 1998 using LiDAR. These two SSW event occasions are also noticed in NCEP data winter 1998–1999 as depicted in Fig. 6.

In Fig. 7a, the HALOE measured temperature profile on 6 December 2006 closely follows the OHP LiDAR observed profile on 5 December 2006 and is comparable with the OHP LiDAR measured temperature on 6 December 2006 with a 2 K degree difference in temperature. In Fig. 7b, the HALOE measured temperature profile on 17 December 1998 is 6 K cooler and closely follows the general trend of the OHP LiDAR measured temperature profile on the same day. The slight difference in magnitude of temperature between OHP LiDAR profile and HALOE profile might be due to the time difference of LiDAR (refer to night time) measurements due to the passage of HALOE satellite (refer to sunset) over OHP.

7 Associated planetary wave activity and large scale transport

7.1 Advection of potential vorticity

To study the atmosphere dynamic related process (say, PW) during the sudden stratospheric warming events, we use isentropic maps of Ertel's Potential Vorticity (EPV). This approach has been followed elsewhere and is used to study SSW in connection with the breaking of planetary waves (e.g. McIntyre and Palmer, 1983; Dunkerton and Delisi, 1986). Their hypothesis suggests that large-scale wave breaking leads to polar-vortex distortion and erosion, and may induce stratospheric warming. Hypothe-

ACPD
7, 15739–15779, 2007

ses made by Dunkerton and Delisi (1986) suggested that the temporal evolution of the size, shape and orientation of the main circumpolar vortex, is clearly revealed by the potential vorticity field. The size of the vortex determines the range of latitudes over which planetary and Rossby waves are able to propagate.

Figure 8a–f shows north polar stereographic projection maps of advected PV (APV) evaluated on the 950-K isentropic surface. These maps were provided by the MIMOSA simulation which were driven by ECMWF-ERA40 reanalysis data for the days 1, 6, 11, 12, 17 and 20 December 1998. The inner and outermost circles designate the 70° N and the Equator respectively. The OHP lidar site is indicated by the symbol "•". Contours of APV values give a well-defined picture of APV gradients and large-scale structures.

The APV map obtained for 1 December 1998 (Fig. 8a) shows a relatively more symmetric and undisturbed vortex over the polar region. Incursion of low-PV values (tropical air-masses) in the shape of a tongue can be seen (see Fig. 8a) over the region with a longitudinal extension from 105° E to 135° E. By 6 December 1998 (during minor SSW event) the incursion of a low-PV caused further extension westward up to 90° W, while high-PV values (polar/vortex air-masses) have tilted and drifted southward over the mid- and subtropical-latitudes, including the OHP location. The spread of the polar air-masses continued on the following days in the form of filamentary structures pulled over in the equator-ward direction. These structures then mixed-up with tropical air-masses, as illustrated by Fig. 8c, d. On 17 December 1998 the polar air-masses almost shifted from high- to mid-latitudes (see Fig. 8e), presumably as a result of the major warming occurrence. On the following days, the high-PV air masses moved further southward and scattered over the mid-latitudes in a shape of a very-large-belt surrounding the low-PV air-masses over polar region (see Fig. 8f).

From a comparison between the minor warming (4–8 December) and the major warming (16–19 December), one observes a significant differences in shape, extent and orientation of the polar vortex. In fact, during the minor warming, the polar vortex keeps relatively symmetric and high-PV air-masses remain located over high-latitude

ACPD
7, 15739–15779, 2007

regions (see Fig. 8b). In contrast, during the major warming, before splitting, the polar vortex is asymmetrically displaced equator-ward and materials are pulled out-off the polar region in the form of filamentary structures as far as tropics/subtropics. This is in good agreement with the arguments concerning the distinction of potential vorticity evolution between major and minor warmings given by McIntyre (1982).

7.2 Planetary wave trajectories: E-P flux

Eliassen-Palm (E-P) flux is used to interpret Planetary Waves (PWs) in terms of propagation and trajectory in the meridional plane. For the present study, wave fluxes in the E-P vector's formulation are calculated using ECMWF ERA-40 reanalysis data. For a clear visualization throughout the stratosphere, the E-P vectors are multiplied by the factor $e^{z/H}$ (Mechoso et al., 1985) and $F_{(Z)}$ is magnified by factor 150 with respect to $F_{(\phi)}$ (Randel et al., 1987). Figure 9 is superimposed on the plot of wave driving (contours), which is proportional to the E-P flux divergence; $D = \frac{1}{\rho_0 a \cos\phi} \nabla . F$.

The Fig. 9a–c shows the meridional cross section of the directions of E-P flux vectors (arrows), calculated for normal winter conditions (no warming day), minor SSW (6 December 1998) and major SSW (17 December 1998). The direction of E-P flux, indicates the active vertical propagation of the wave flux, for planetary waves propagating from one height and latitude to another. During a normal winter (see Fig. 9a), one notices that the E-P arrows in the low latitude upper troposphere have strong equatorward components. The length of E-P arrows in the stratosphere is small, indicating that the values are less. Figure 9b, c shows E-P cross-section for the days of minor and major SSWs observed on 6 and 17 December 1998. On 6 December 1998, strong upward and equatorward movement appeared in the mid-latitude, upper stratosphere region and the length of E-P flux values are higher than those on the day of no warming (see Fig. 9a). On 17 December 1998, one can see strong upward movement in the mid-latitude, upper stratosphere as well as in the lower stratosphere. While a positive $\nabla * \bullet E$ region in the middle latitude troposphere, indicates the source of momentum in

that region.

It is evident from the figure, that the OHP LiDAR has observed minor and major warmings (see Fig. 6b and c) over OHP (44° N) that occurred at ~46 km and ~40 km respectively. It is well interpreted by the E-P flux analysis, in Fig. 9b and c, that for minor and major warmings over 44° N region, the "focusing" of the waves is mostly around 40 km and 35 km respectively. On 6 December, the day of the minor warming over OHP, the wave propagation is towards the equator and tropical region which differs from the situation on major warming day, where the wave propagation mostly "focuses" over mid-latitude region.

It is interesting to see the strong E-P flux which exists on the day of minor warming. The direction of E-P flux is equator-ward and towards the tropical region, where the stronger wave activity and convergence of E-P flux are likely to produce rapid deceleration of zonal-mean zonal wind and the associated increase in temperature. It can be interpreted that this situation might have lead to a major warming (e.g. McIntyre 1982). On 17 December, the day of major warming, the "focusing" of the waves, at around 30 km to 35 km over 44° N latitude region, and the zonal mean wind reversal (shaded and contours) exists exactly over the region where the OHP is located. On 25 December 1998, as an example for a "no warming" day (Fig. 9a), the middle atmosphere returns to normal, with planetary-wave activity remarkably weaker in the stratosphere region.

8 SSW: Statistical characteristics

8.1 SSW general characteristics

Twenty years of night-time quasi-continuous Rayleigh LiDAR temperature data is used to obtain the statistical characteristics of SSW events that were observed over OHP. The characteristics, listed in the Table 1, are provided in terms of dates of occurrence, descent of stratopause, magnitude of temperatures, types of warming (major/minor)

and occurrence of SSWs in relation with the phase of QBO. The following are the main salient features obtained from the statistical study;

- There are 43 SSW events recorded in winter months (NDJFM). Among 43 SSW events, 10 events are major warmings and 33 events are minor warmings.
- Among 10 major warmings, 4 major warmings are followed by minor warmings and 2 are preceded by minor warmings during the yearly winter (NDJFM) period.
- Among 43 events, the number of occurrences of SSWs are 2, 15, 12, 8 and 6, respectively in November, December, January, February and March. Out of 10 major events, none were observed in November, 2 events observed in December and January respectively, 3 events observed in February and March repsectively. Similarly, the 33 minor events are distributed as follows: 2, 13, 10, 5 and 3 in November, December, January, February and March repsectively.
- The decent of stratopause with respect to winter mean stratopause height, was varied from 1 km to 6 km, for major warmings and from 0 km to 6 km in the case of minor warmings. The mean decent of height is ~1.2 km for major warming and ~5.3 km for minor warming.
- The magnitude of warmings with respect to the overall winter temperature profile, varied from 12.2 K to 35.7 K for major warmings and from 10.2 K to 32.8 K in the case of minor warmings. On average, the magnitude of the warm temperature is noted as ~20.1 K for major warming and ~18.8 K for minor warming.

9 Distribution of SSWs in relation with QBO phase

Although the QBO is a tropical phenomenon, it affects the stratospheric flow from pole to pole (Baldwin et al., 2001) and it dominates the zonal wind in the tropical stratosphere (e.g., Naujokat, 1986). Thereafter, a suggestion was made by McIntyre (1982)

ACPD
7, 15739–15779, 2007

that deep equatorial easterlies may favor the occurrence of a strong mid-winter warming and that SSWs tend to occur more frequently during the easterly phase of the equatorial QBO than the westerly phase (Labitzke, 1982). Dunkerton (1988) studied the occurrence of major SSWs in relation to QBO by using 35 years of satellite data. Their study suggested that Northern Hemisphere winter major SSWs have not occurred when the equatorial monthly mean zonal winds are deep westerly. And more than half of the major SSWs have occurred when the equatorial flow is easterly at 10 and 50 hpa levels. In order to study the apparent connection between the QBO and SSW, particularly to study the distribution of major or minor warming in relation with QBO phase and in future to determine how much a particular warming contributes to interannual variability, we use the QBO data documented by Naujokat (1986), which is developed by using monthly averages of rawinsonde observations at Singapore (1° N, 103° E), as well as two other stations (Canton Island (2.46° S, 171.43° W), Gan/Maledives (0.41° S, 73.09° E)) for earlier years. They are available at 10, 15, 20, 30, 40, 50 and 70 hPa.

Using the above 20 years of SSW statistics (see Table 1) and the monthly mean zonal wind at a 10 hPa pressure level (see Fig. 10), the frequency of occurrence of major and minor warming in relation to QBO phase is summarized as follows;

- Among a total of 43 SSW events, 23 events are observed when QBO is in east phase, 18 events are observed when QBO is in west phase and remaining 2 events are observed when the QBO is in the transitional phase between east/west or west/east.
- Among 10 major SSW events, 5 events are observed when the QBO is in east phase, 4 events are observed when the QBO phase is in west phase and 1 event is observed in the transitional phase.
- Among 33 minor SSW events, 18 events are observed when the QBO is in east phase, 14 events are observed when the QBO phase is west and 1 event is observed when the QBO is in the transitional phase.

– When the QBO phase is west, maximum warm temperature and maximum descent of stratopause is observed as 28.8 K and ∼6 km respectively; whereas when QBO phase is east, the maximum warm temperature and maximum descent of stratopause observed is 35.7 K and ∼6 km respectively.

Table 1 presents the statistical characteristics of SSWs which were observed over a mid-latitude site in the Northern Hemisphere (OHP). The SSWs occurred in 20 sequential winter seasons (November to March) and their classifications are presented. With the objective of classifying them into major and minor warmings, the correlation of occurrence between the onset dates of warming events in the NCEP and OHP data sets, to the dates of occurrence of SSW events noticed in OHP LiDAR data is observed. Only the nearest available dates of onset of circulation reversal (westerly to easterly) is noticed in the NCEP data (zonal mean temperature at 80° N and zonal mean wind at 60° N at 10-hPa pressure level) and are presented in the first column of Table 1. Note that the onset dates of circulation reversal observed in NCEP data during winters 1990/1991, 1992/1993 and 1996/1997 are not presented in the first column of Table 1. In the second column, we report the dates of occurrence of 42 SSW events, during the above mentioned period noticed in the OHP LiDAR data, and their classification using the usual criteria (see Sect. 4a) as either a major (M) or minor (m) SSW event. In the second column, the "+" sign or "–" sign is together displayed with either an "M" or "m" which denotes the phase state of QBO ("+" denotes west and "–" denotes east phase) during a major (M) or minor (m) warming event. In columns 3 to 6, the statistical characteristics of noticed SSWs, such as magnitude of warm temperature (ΔT), warm stratopause height, mean winter stratopause height and descent of stratopause, in OHP lidar data, are presented respectively. In the winter of 1981/1982 (using lidar data since 1 January 1982), two SSW events are noticed; the first one occurred on 2 February 1982 and the second on 31 March 1982. Figures 2 and 4 of Hauchecorne and Chanin (1983) shows a "strong minor warming" that has commenced on 2 February (earliest date of onset) over OHP, which has been classified as a minor warming event. The event observed on 31 March 1982 was not reported by Hauchecorne and

ACPD
7, 15739–15779, 2007

Chanin (1983), even though a NCEP observation is made earlier. Based on Naujokat and Labitzke (1993), we have classified this event as a major warming. In winter 1982/1983, four warming occasions were noticed at the end of December and at the end of January. Among the four occasions, based on circulation reversal observed on 17 December 1982 in NCEP data, the event observed on 22 December 1982 is classified as a major warming and the remaining three events were classified as minor warmings. In winter 1983/1984, among the three warming events observed in the early winter, end of February and beginning of March, the events noticed on 9 November and 4 March (based on NCEP observation) were classified as minor and major warmings respectively. In the case of event observed on 23 February, the NCEP observations show circulation reversal one day later to the SSW observed over OHP and based on Naujokat and Labitzke (1993), the event is therefore classified as a major SSW. In winter 1984/1985, four warming events were noticed in the beginning of December, beginning of January and in the middle of March. Based on NCEP observations till the end of December, the events observed on 4 and 11 of December were classified as minor warmings, but the event observed (over OHP) on 4 December was reported as a Canadian warming for the same day by Naujokat and Labitzke (1993). The event observed on 1 January is also reported by them as major mid winter warming. Based on NCEP observations, it is classified as major warming. The event observed on 14 March was reported as a final warming by them. Based on NCEP observations during February and March, it is classified as a minor warming. During winter 1985/1986, no circulation reversal was observed in NCEP data, hence the event noticed on 27 November is classified as a minor warming. In winter 1986/1987, six warming events were observed during December, January, end of February and the end of March. Based on zonal wind circulation reversal in NCEP data observed from 23 to 27 January and 21 to 24 February, the events of 1 and 23 December, 4 January and 24 March events were classified as minor warmings and the events observed on 23 January (Manney et al., 2005) and 27 February has been classified as major warmings. All events observed during winter 1987/1988 to 1997/1998 were classified as minor warmings based on the

ACPD
7, 15739–15779, 2007

fact that no wind reversal was observed in the NCEP data. In winter 1998/1999, four events were observed in December and January and based on NCEP observations of wind reversal noticed on 15 to 21 December, the event observed on 17 December is classified as major warming. The same event was reported by Manney et al. (1999) for the day of 15 December. The remaining events of 6 December, 7 and 14 January were classified as minor warming. In winter 1999/2000, four warming events were found during the end of December, beginning of February and the end of March based on the onset of wind reversal observed in NCEP data on 21 March. Among the events of 22 and 30 December, 4 February and 27 March, the event observed on 27 March was classified as a major warming and the remaining three events were classified as minor warmings. In winter 2000/2001, one event was observed on 15 February (Jacobi et al., 2003) and was classified as a major warming based on the circulation reversal observed on 12 to 23 February in NCEP data.

The magnitude of maximum temperature is observed in the order of 270–280 K over the stratopause region at 40 to 60 km. The magnitude of maximum warm temperature observed over OHP (mid-latitude station) is 35.7 K, which is comparable with the warm temperatures observed, thus far, over mid- and high-latitude stations (about 30 K) (Hauchecorne and Chanin, 1983; Whiteway and Carswell, 1994; Whiteway et al., 1997; Duck et al., 1998). Using EP flux calculations from ECMWF ERA 40 data, it was found that the SSW was mainly due to PW propagation from high to mid latitudes, consecutive to the warming episode over pole.

10 Conclusions

This paper reports the statistical characteristics of SSWs observed over a mid-latitude station (OHP, South of France) for the first time using 20 years (starting from 1 January 1982 to 6 November 2001) of Quasi-continuous LiDAR nighttime temperature data. Statistically, most of the OHP observed events, are in good agreement with the NCEP, ECMWF-ERA 40 and HALOE data sets. There are a few exceptions observed in the

ACPD
7, 15739–15779, 2007

SSW data sets when compared with the NCEP data. Here, it was noticed that some events occur a day earlier to the events observed in the other (OHP, ECMWF and HALOE) data sets.

SSWs occur with a mean frequency of 2.15 events per winter season. Out of 20 sequential winters starting from winter 1981/1982 to 2000/2001, 8 winters have had occurrences of major warmings and 17 winters have had occurrences of minor warmings. In total, 43 warming events have been identified. Among them, 10 events (about ~23%) are major warmings and 33 events (about ~77%) are minor warmings. The maximum-minimum magnitude of the warm temperatures, observed for the major and minor warmings, are in the range of 35.7–12.2 K and 32.8–10.2 K respectively. Also associated with major and minor warmings, the descent of stratopause layer by −4 to 6 km and −6 to 6 km respectively, is observed.

As a case study on winter 1998/1999, using the MIMOSA simulated APV evolution (Hauchecorne et al., 2002) and EP flux calculations based on ECMWF reanalysis, we found that the minor and major warming episodes are mainly attributed to the transport of tropical/polar air masses from high- and mid- to low-latitudes caused by Planetary Waves as a consecutive to the major warming episode over the polar region.

Among the total of 43 SSW events, 23 have occurred when the QBO phase was east and 18 have occurred when QBO phase was west. The remaining 2 events occurred when the QBO was in the transitional phase (east/west).

In the case of major warmings, the maximum magnitude of warm temperature was observed when the QBO phase was east, but in the case of minor warming the maximum magnitude of warm temperature was observed when the QBO phase was west. The minimum magnitude of warm temperatures observed for the both major and minor warmings is when the QBO phase was east. The quasi-periodic behavior of temperature with variations of 2 to 3 year periods is probably associated with the QBO.

However, the maximum warm temperatures for the both the major and minor warmings are observed when the QBO phase was east. Since the main objective of this present paper is to report the observed statistical characteristics of SSW, we briefly

ACPD
7, 15739–15779, 2007

discuss the dynamical process during the SSW occurrence in Sect. 4b (i) and (ii).

Finally, a table of observed statistical characteristics of SSWs is compiled. These benchmarks maybe used in future to contribute to modelling studies and to study the expected features of planetary wave propagation during SSWs. Further, we are interested in using primarily ground based LiDAR data in the Northern and Southern hemispheres to study and define the characteristics of SSW events which are observed at different low and mid-latitudes.

Acknowledgements. The Laboratoire de l'Atmosphère et des Cyclones (LACy) is supported by the French Centre National de la Recherche Scientifique (CNRS)/Institut National des Sciences de l'Univers (INSU) and the Conseil Régional de la Réunion. The authors wish to thank NOAA Climate Diagnostics Center (http://www.cdc.noaa.gov/) for providing portions of the NCEP data. The authors would like to thank the Goddard Space Flight Center, for providing HALOE satellite data through their web site http://haloedata.larc.nasa.gov/home/index.php. The authors are thankful to the European Centre for Medium-Range Weather Forecasts for providing portions of ECMWF-ERA40 reanalysis data through their web (http://www.ecmwf.int/research/era/). One of the authors, D. V. Acharyulu, acknowledges the Conseil Régional de la Réunion for financial support under the PhD fellowship scheme. The authors are thankful to A. Sharma for reading the manuscript and improving the readability.

References

Andrews, D. G., Holton, J. R., and Leovy, C. B.: Middle Atmosphere Dynamics, Academic Press, 1985.

Appu, K. S.: On Perturbation in the Thermal structure of tropical Stratosphere and Mesosphere in Winter, Indian J. Radio Space, 13, 35–41, 1984.

Baldwin, M. P. and Dunkerton, T. J.: The stratospheric major warming of early December 1987, J. Atmos. Sci., 46, 2863–2884, 1989.

Baldwin, M. P. and Dunkerton, T. J.: Downward propagation of the Arctic Oscillation from the stratosphere to the troposphere, J. Geophys. Res., 104, 937–946, 1999.

Baldwin, M., Gray, L. J., and Dunkerton, T. J.: The Quasi-Biennial Oscillation, Rev. Geophys., 39, 179–229, 2001.

Baldwin, M. P., Hirooka, T., O'Neill, A., Yoden, S., Charlton, A. J., Hio, Y., Lahoz, W. A., and Mori, A.: Major stratospheric warming in the southern hemisphere in 2002: dynamical aspects of the ozonehole split, SPARC Newsletter, 20, 24–26, 2003.

Chanin, M. L. and Hauchecorne, A.: Lidar studies of temperature and density using Rayleigh scattering, in: Handbook for MAP: Ground-Based Techniques, edited by: Vincent, R. A., 13, 7, Scientific Committee on Solar Terrestrial Physics, International Council of Scientific Unions, Urbana, IL. 1984.

Delisi, D. P. and Dunkerton, T. J.: Seasonal variation of the semiannual oscillation, J. Atmos. Sci., 45, 2772–2787, 1988.

Donfrancesco, G., Adriani, A., Gobbi, G. P., and Congeduti, F.: Lidar observations of stratospheric temperatures above McMurdo Station (78 S, 167 E), Antarctica , J. Atmos. Terr. Phys., 58, 1391–1399, 1996.

Duck, T. J., Whiteway, J. A., and Carswell, A. I.: Lidar observations of gravity wave activity and Arctic stratospheric vortex core warming, Geophys. Res. Lett., 25, 2813–2816, 1998.

Dunkerton, T. J. and Delisi, D. P.: Evolution of potential vorticity in the winter stratosphere of January–February 1979, J. Geophys. Res., 91, 1199–1208, 1986.

Dunkerton, T. J., Delisi, D. P., and Baldwin, M. P.: Distribution of major stratospheric warmings in relation to the quasi-biennial oscillation, Geophys. Res. Lett., 15, 136–139, 1988.

Dunkerton, T. J. and Baldwin, M. P.: Quasi-biennial Modulation of Planetary-Wave Fluxes in the Northern Hemisphere Winter, J. Atmos. Sci., 48, 1043–1061, 1991.

Hansen, J., Russell, G., Rind, D., Stone, P., Lacis, A., Lebedeff, S., Ruedy, R., and Travis, L.: Efficient three-dimensional global models for climate studies: Models I and II, Mon. Weather Rev., 111, 609–662, 1983.

Hauchecorne, A. and Chanin, M. L.: Density and temperature profiles obtained by lidar between 35 and 70 km, Geophys. Res. Lett., 8, 565–568, 1980.

Hauchecorne, A. and Chanin, M. L.: Mid latitude observations of planetary waves in the middle atmosphere during the winter over 1981–1982, J. Geophys. Res., 88, 3843–3849, 1983.

Hauchecorne, A., Chanin, M. L., and Keckhut, P.: Climatology and trends of the middle atmospheric temperature (33–87 KM) as seen by Rayleigh LiDAR over the South of France, J. Geophys. Res., 96(D8), 15 297–15 309, 1991.

Hauchecorne, A., Godin, S., Marchand, M., Heese, B., and Souprayen, C.: Quantification of the transport of chemical constituents from the polar vortex to midlatitudes in the lower stratosphere using the high-resolution advection model MIMOSA and effective diffusivity, J.

Geophys. Res., 107(D20), 8289, doi:10.1029/2001JD000491, 2002.
Heese, B., Godin, S., and Hauchecorne, A.: Forecast and simulation of stratospheric ozone filaments: A validation of a high-resolution PV advection model by airborne ozone lidar measurements in winter 1998–1999, J. Geophys. Res., 106(D17), 20 011–20 024, 2001.
Hervig, M. E., Russell III, M., Gordley, L. L., Drayson, S. R., Stone, K., Thompson, E., Gelman, M. E., and McDermid, I. S.: A validation of temperature measurements from the Halogen occultation Experiment, J. Geophys. Res., 101(D6), 10 277–10 286, 1996.
Holton, J. R., Pyle, J. A., and Curry, J. A.: Encyclopedia of Atmospheric Sciences, Elsevier, 1342–1353, 2002.
Holton, J. R. and Austin, J.: The influence of the QBO on sudden stratospheric warmings, J. Atmos. Sci., 48, 607–618, 1991.
Jacobi, C., Kurschner, D., Müller, H. G., Pancheva, D., Mitchell, N. J., and Naujokat, B.: Response of the mesopause region dynamics to the February 2001 stratospheric warming, J. Atmos. Terr. Phys., 65, 843–855, 2003.
Kalnay, E., Kanamitsu, M., Kistler, R., Collins, W., Deaven, D., Gandin, L., Iredell, M., Saha, S., White, G., Woollen, J., Zhu, Y., Chelliah, M., Ebisuzaki, W., Higgins, W., Janowiak, J., Mo, K., Ropelewski, C., Wang, J., Leetmaa, A., Reynolds, R., Jenne, R., and Joseph, D.: The NCEP/ NCAR 40-year re-analysis project, B. Am. Meteorol. Soc., 77, 437–471, 1996.
Kanzawa, H.: Four observed sudden stratospheric warmings diagnosed by the Eliassen-Palm flux and refractive index, Dynamics of the Middle Atmosphere, in: Proceedings of a U.S.-Japan Seminar, Honolulu, Hawaii, 8–12 November, 1982, edited by: Holton, J. R. and Matsuno, T., 307–331, 1984.
Labitzke, K.: Inter-annual variability of the winter stratosphere in the northern hemisphere, Mon. Weather Rev., 105, 762–770, 1977.
Labitzke, K.: Stratospheric-mesospheric midwinter disturbances: a summary of observed characteristics, J. Geophys. Res., 86, 9665–9678, 1981.
Labitzke, K.: The amplification of height wave 1 in January 1979: A characteristic precondition for the major warming in February, Mon. Weather Rev., 109, 983–989, 1981.
Labitzke, K., Lenschow, R., Naujokat, B., and Petzoldt, K.: First information on the major mid-winter warming in February 1981, Beilage zur Berliner Wetterkarte, SO 4/81, 1981.
Labitzke, K.: On the interannual variability of the middle stratosphere during the northern winters, J. Meteorol. Soc. Jpn., 60, 124–139, 1982.
Labitzke, K.: Sunspots, the QBO, and the stratospheric temperature in the north polar region,

Geophys. Res. Lett., 14, 535–537, 1987.
Labitzke, K. and van Loon, H.: The Stratosphere-Phenomena, History, and Relevance, Springer, Berlin, 1999.
Labitzke, K. and Kunze, M.: Stratospheric temperatures over the Arctic: Comparison of three data sets, Meteorolog. Z., 14, 65–74, 2005.
Leblanc, T., McDermid, I. S., She, C. Y., Krueger, D. A., Hauchecorne, A., and Keckhut, P.: Temperature climatology of the middle atmosphere from long-term lidar measurements at mid- and low-latitudes, J. Geophys. Res., 103, 17 191–17 204, 1998.
Limpasuvan, V., Thompson., D. W. J., and Hartmann, D. L. : The life cycle of Northern Hemisphere sudden stratospheric warmings, J. Climate, 17, 2584–2596, 2004.
Lorenz, E. N.: The nature and theory of general circulation of the atmosphere, No. 218, 161 pp., World Meteorological Organization, Geneva, 1967.
Manney, G. L., Kruger, K., Sabutis, J. L., Sena, S. A., and Pawson, S.: The remarkable 2003–2004 winter and other recent warm winters in the Artic stratosphere since the late 1990s, J. Geophys. Res., 100, doi:10.1029/2004JD006367, 2005.
Manney, G. L., Lahoz, W. A., Swinbank, R., O'Neill, A., Connew, P. M., and Zurek, R. W.: Simulation of the December 1998 stratospheric major warming, Geophys. Res. Lett., 26, 2733–2736, 1999.
Marchand, M., Godin, S., Hauchecorne, A., Lefévre, F., Bekki, S., and Chipperfield, M.: Influence of polar ozone loss on northern mid-latitude regions estimated by a high-resolution chemistry transport model during winter 1999/2000, J. Geophys. Res., 108(D5), 8326, doi:10.1029/2001JD000906, 2003.
Marenco, F., Santacesaria, V., Bais, A., Balis, D., di Sarra, A., Papayannis, A., and Zerefos, C. S.: Optical properties of tropospheric aerosols determined by lidar and spectrophotometric measurements (PAUR campaign), Appl. Opt., 36, 6875–6886, 1997.
Matsuno, T.: A dynamical model of the stratospheric sudden warming, J. Atmos. Sci., 28, 1479–1494, 1971.
McIntyre, M. E.: How well do we understand the dynamics of stratospheric warmings?, J. Meteorol. Soc. Jpn., 60, 37–65, 1982.
McIntyre, M. E. and Palmer, T. N.: Breaking planetary waves in the stratosphere, Nature, 305, 593–600, 1983.
Mechoso, C. R., Hartmann, D. L., and Farrara, J. D.: Climatology and interannual variability of wave, mean-flow interaction in the Southern Hemisphere, J. Atmos. Sci., 42, 2189–2206,

1985.
Morel, B., Bencherif, H., Keckhut, P., Portafaix, T., Hauchecorne, A., and Baldy, S.: Fine-scale study of a thick stratospheric ozone lamina at the edge of the southern subtropical barrier: 2. Numerical simulations with coupled dynamics models, J. Geophys. Res., 110, D17101, doi:10.1029/2004JD005737, 2005.
Naujokat, B.: An update of the observed quasi-biennial oscillation of the stratospheric winds over the tropics, J. Atmos. Sci., 43, 1873–1877, 1986.
Naujokat, B. and Labitzke, K.: Collection of reports on the stratospheric circulation during the winters 1974/75–1991/92, STEP Handbook, July 1993, SCOSTEP Urbana, Illinois, USA, 1993.
Naujokat, B., Krüger, K., Matthes, K., Hoffmann, J., Kunze, M., and Labitzke, K.: The early major warming in December 2001 – exceptional?, Geophys. Res. Lett., 29, doi:10.1029/2002GL015316, 2002.
Nee, J. B., Thulasiraman, S., Chen, W. N., VenkatRatnam, M., and Narayana Rao, D.: Middle atmospheric temperature structure over two tropical locationas, Chung Li (25° N,121° E) and Gadanki (13.5° N,79.2° E), J. Atmos. Sol.-Terr. Phy., 64, 1311–1319, 2002.
O'Neill, A. and Taylor, B. F.: Study of the major stratospheric warming of 1976–77, Quart. J. Roy. Meteor. Soc., 105, 75–92, 1979.
O'Neill, A.: Stratospheric Sudden Warmings, Encyclopedia of Atmospheric Sciences, 1342–1353, 2003.
Quiroz, R. S., Miller, A. J., and Nagatani, R. M.: A comparison of observed and simulated properties of sudden stratospheric warmings, J. Atmos. Sci., 32, 1723–1736, 1975.
Quiroz, R. S.: The tropospheric-stratospheric polar vortex breakdown of January 1977, Geophys. Res. Lett., 4, 151–154, 1977.
Quiroz, R. S.: The association of stratospheric warmings with tropospheric blocking, J. Geophys. Res., 91, 5277–5285, 1986.
Randel, W. J. and Boville, B. A.: Observations of Major Stratospheric Warming during December 1964, J. Atmos. Sci., 44, 2179–2186, 1987.
Randel, W., Fleming, E., Geller, M., Gelman, M., Hamilton, K., Karoly, D., Ortland, D., Pawson, S., Swinbank, R., Udelhofen, P., Wu, F., Baldwin, M., Chanin, M.-L., Keckhut, P., Labitzke, K., Remsberg, E., Simmons, A., and Wu, D.: The SPARC Intercomparison of Middle Atmosphere Climatologies, WCRP – 116, WMO/TD-No. 1142, SPARC Report No. 3, December, 2002.

Roble, R. G. and Dickinson, R. E.: How will changes in carbon dioxide and methane modify the mean structure of the mesosphere and thermosphere?, Geophys. Res. Lett., 16, 1441–1444, 1989.

Scherhag, R.: Die explosionsartigen Stratosphärenerwärmungen des Spätwinters 1951/52. Berichte des deutschen Wetterdienstes in der US-Zone, 6, 38, 51–63, 1952.

Schoeberl, M. R.: Stratospheric warmings: Observations and theory, Rev. Geophys. Space. Phys., 16, 521–538, 1978.

Sivakumar, V., Rao, P. B., and Krishnaiah, M.: Lidar studies of Stratosphere-Mesosphere Thermal Structure over Low Latitude: Comparison with satellite and models, J. Geophys. Res., 108(D11), 4342, doi:10.1029/2002JD003029, 2003.

Sivakumar, V., Morel, B., Bencherif, H., Baray, J. L., Baldy, S., Hauchecorne, A., and Rao, P. B.: Rayleigh lidar observation of a warm stratopause over a tropical site, Gadanki (13.5° N; 79.2° E), Atmos. Chem. Phys., 4, 1989–1996, 2004, http://www.atmos-chem-phys.net/4/1989/2004/.

Sivakumar, V., Bencherif, H., Hauchecorne, A., Keckhut, P., Narayana Rao, D., Sharma, S., Chandra, H., Jayaraman, A., and Rao, P. B.: Rayleigh lidar observations of double stratopause structure over three different northern hemisphere stations, Atmos. Chem. Phys. Discuss., 6, 6933–6956, 2006, http://www.atmos-chem-phys-discuss.net/6/6933/2006/.

Walterscheid, R. L., Sivjee, G., and Roble, R. G.: Mesospheric and lower thermospheric manifestations of a stratospheric warming event over Eureka, Canada (80° N), Geophys. Res. Lett., 27, 2897–2900, 2000.

Whiteway, J. A. and Carswell, A. I.: Rayleigh Lidar Observations of Thermal Structure and Gravity Wave Activity in the High Arctic during a Stratospheric Warming, J. Atmos. Sci., 51, 3122–3136, 1994.

Whiteway, J. A., Duck, T. J., Donovan, D. P., Bird, J. C., Pal., S. R., and Carswell, A. I.: Measurements of gravity wave activity within and around the Arctic stratospheric vortex, Geophys. Res. Lett., 24, 1387–1390, 1997.

Table 1. Statistics of SSW events observed over OHP.

Date of SSW observed		ΔT	Height (km)			Reference
NCEP	OHP	(K)	SSW	S_w	S_d	
4 to 6 Dec 1981	2 Jan 1982 $^{-.m}$	11.0	50	50	0	Hauchecorne and Chanin (1983)
	31 March 1982 $^{+.M}$	18.1	54	50	−4	Naujokat and Labitzke (1993)
17 Dec 1982	22 Dec 1982 $^{+.M}$	15.2	45	47	2	-do-
	28 Dec 1982 $^{+.m}$	19.4	46	47	1	
	21 Jan 1983 $^{+.m}$	14.6	48	47	−1	-do-
	28 Jan 1983 $^{+.m}$	17.9	47	47	0	
	09 Nov 1983 $^{-.m}$	12.7	47	47	0	Naujokat and Labitzke (1993)
24 to 27 Feb 1984	23 Feb 1984 $^{-.M}$	15.8	46	47	1	
01 to 31 March 1984	04 March 1984 $^{-.M}$	14.5	45	47	2	
	4 Dec 1984 $^{+.m}$	10.2	44	44	0	Randel and Boville (1987)
	11 Dec 1984 $^{+.m}$	13.0	43	44	1	-do-
1 to 5 Jan 1985	1 Jan 1985 $^{+.M}$	22.0	38	44	6	
	14 March 1985 $^{+.m}$	11.7	42	44	2	
	27 Nov 1985 $^{-.m}$	17.3	50	49	−1	
	1 Dec 1986 $^{-.m}$	14.1	47	47	0	Manney et al. (2005)
	23 Dec 1986 $^{-.m}$	19.2	48	47	−1	
	4 Jan 1987 $^{-.m}$	17.7	42	47	5	
23 to 27 Jan 1987	23 Jan 1987 $^{-.M}$	35.7	43	47	4	
21 to 24 Feb 1987	27 Feb 1987 $^{-.M}$	12.2	41	47	6	
	24 March 1987 $^{-.m}$	11.0	48	47	−1	
	21 Feb 1988$^{-.m}$	18.7	54	49	−5	Baldwin and Dunkerton (1989)
	17 Dec 1988 $^{-.m}$	32.8	46	49	3	
	5 Jan 1989 $^{-.m}$	19.3	46	49	3	
	5 Jan 1990 $^{+.m}$	21.8	46	47	1	Hauchecorne at al. (1991)
	9 Feb 1990 $^{+.m}$	17.2	46	47	1	
	5 Dec 1991 $^{-.m}$	11.1	49	48	−1	
	15 Dec 1991 $^{+/-.m}$	27.0	43	48	5	
	15 Jan 1992 $^{+.m}$	16.6	47	48	1	
	12 March 1992 $^{+.m}$	10.3	47	48	1	
	7 Feb 1994 $^{-.m}$	20.0	49	48	−1	
	13 Jan 1995 $^{+.m}$	28.8	44	48	4	
	18 Dec 1995 $^{-.m}$	24.0	48	49	1	
	15 Feb 1996 $^{-.m}$	21.3	43	49	6	
	3 Dec 1997 $^{-.m}$	32.2	54	48	−6	
	6 Dec 1998 $^{+.m}$	15.1	46	46	0	Manney et al. (1999)
15 to 21 Dec 1998	17 Dec 1998 $^{+.M}$	28.7	40	46	6	
	7 Jan 1999 $^{+.m}$	18.1	44	46	2	
	14 Jan 1999 $^{+.m}$	14.4	43	46	3	
	22 Dec 1999 $^{-.m}$	17.9	45	48	3	
	30 Dec 1999 $^{-.m}$	26.5	45	48	3	
	4 Feb 2000 $^{-.m}$	17.3	47	48	1	
21, 22 March 2000	27 March 2000 $^{-.M}$	19.1	44	48	4	
12 to 23 Feb 2001	15 Feb 2001 $^{+/-.M}$	15.6	44	47	3	Jacobi et al. (2003)

Where, +/− stands for QBO phase west/east; M – Major warming (10), m – minor warming (33), S_w and S_d indicates the winter stratopause and descent of stratopause height.

ACPD
7, 15739–15779, 2007

EGU

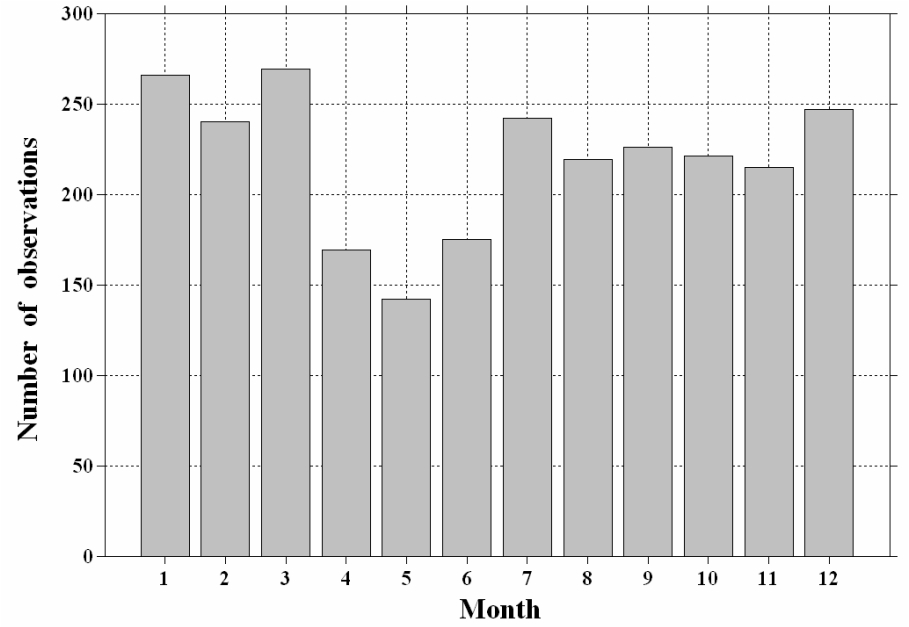

Fig. 1. Monthly distribution of number of OHP lidar observations used from 1 January 1982 to 6 November 2001.

ACPD
7, 15739–15779, 2007

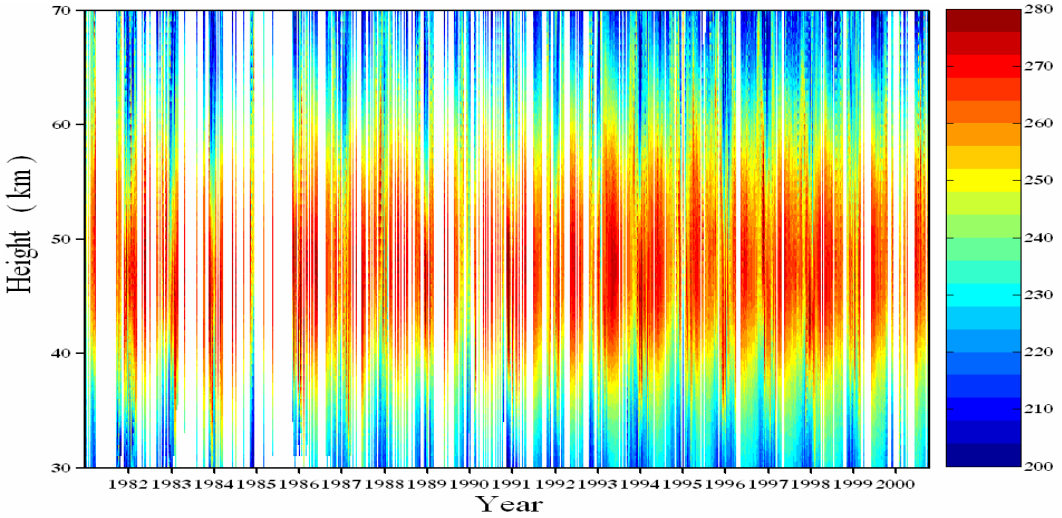

Fig. 2. Temporal evolution of temperature observed from 1 January 1982 to 6 November 2001, the blank space in the figure indicates actual data gap.

ACPD

7, 15739–15779, 2007

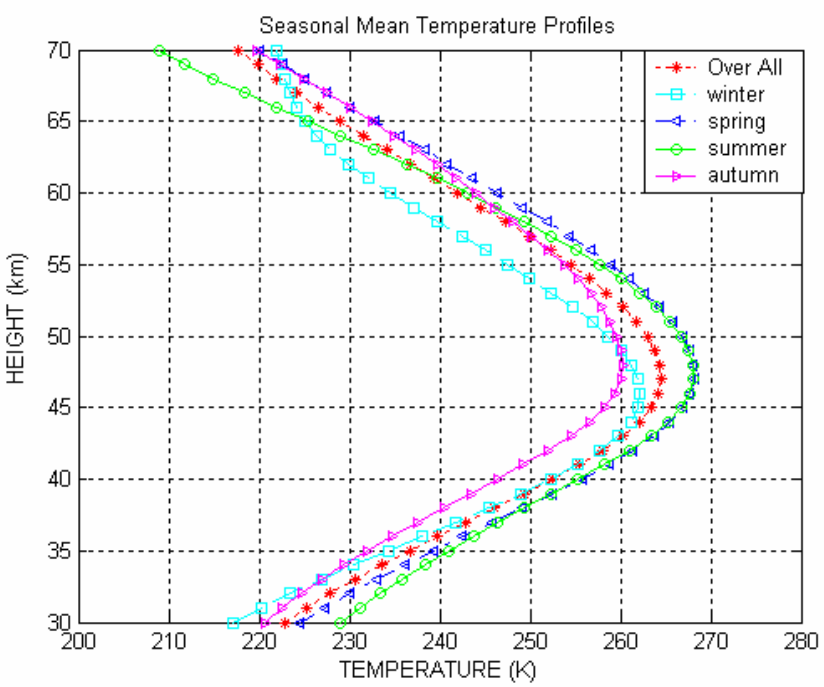

Fig. 3. Seasonal mean temperature profiles obtained from the data during the year 1982 to 2001.

ACPD
7, 15739–15779, 2007

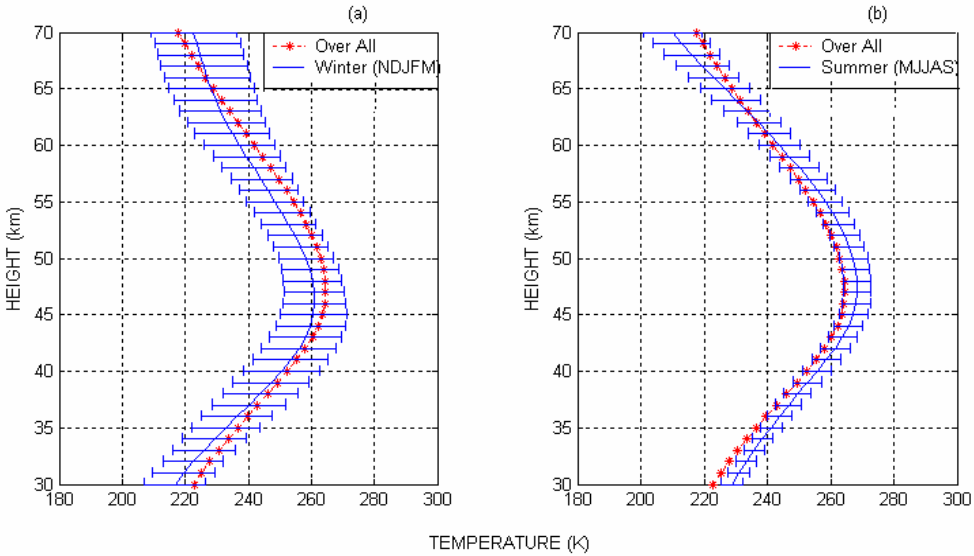

Fig. 4. Over-all mean and seasonal temperature profile during **(a)** winter and **(b)** summer along with the standard deviations obtained from the data during the year 1982 to 2001. The standard deviation is shown for the seasonal temperature profile.

ACPD
7, 15739–15779, 2007

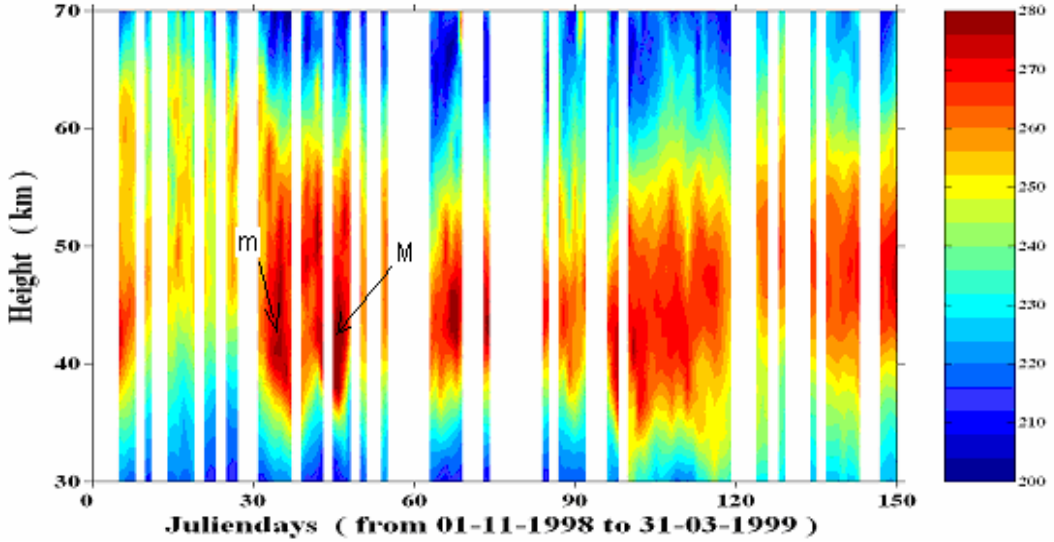

Fig. 5. Time evolution of OHP temperature starting from 1 November 1998 to 31 March 1999, "m" – minor SSW (6 December 1998), "M" – major SSW (17 December 1998).

ACPD

7, 15739–15779, 2007

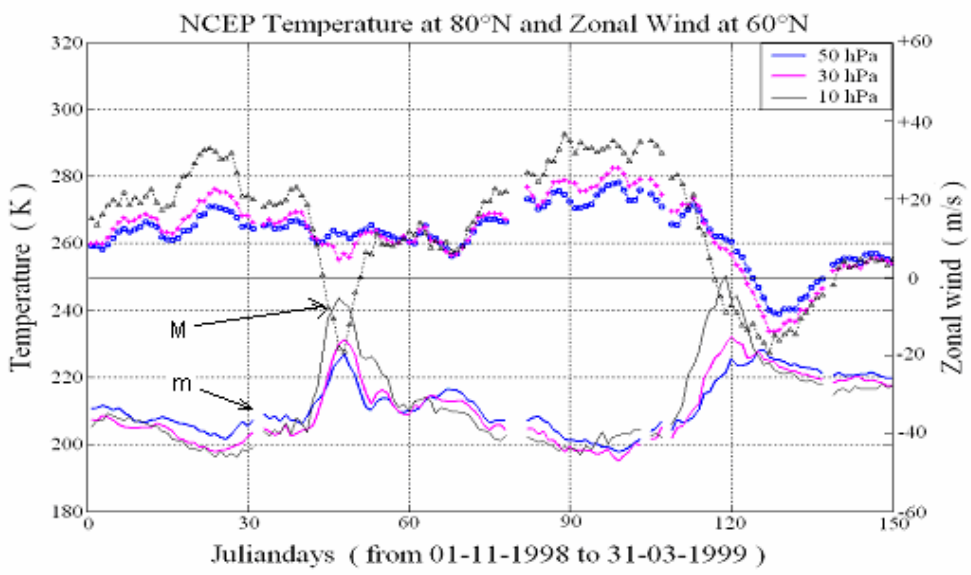

Fig. 6. Time evolution of NCEP data of zonal-mean temperature at 80° N and zonal mean wind at 60° N at 50, 30 and 10 hPa level during 1 November 1998 to 31 March 1999. The solid line denotes temperature and the line with legend denotes wind. "m" – minor SSW (6 December 1998), "M" – major SSW (17 December 1998).

ACPD
7, 15739–15779, 2007

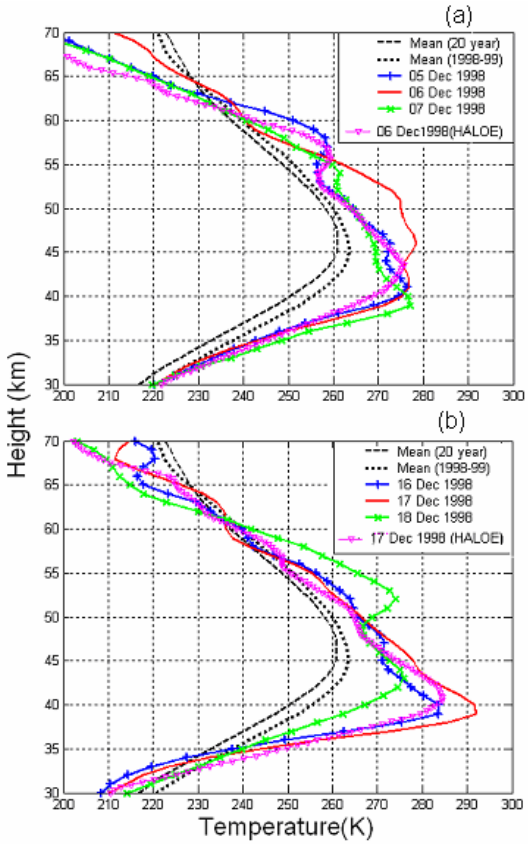

Fig. 7. Height profile of temperature for the first **(a)** and the second **(b)** warming occasions observed during 4–8 December 1998 and 16–19 December 1998. The overall and yearly mean profiles are superimposed in the same figure (see, Legend). The HALOE temperature measurements corresponds to the same day and overpass near to OHP lidar station.

ACPD
7, 15739–15779, 2007

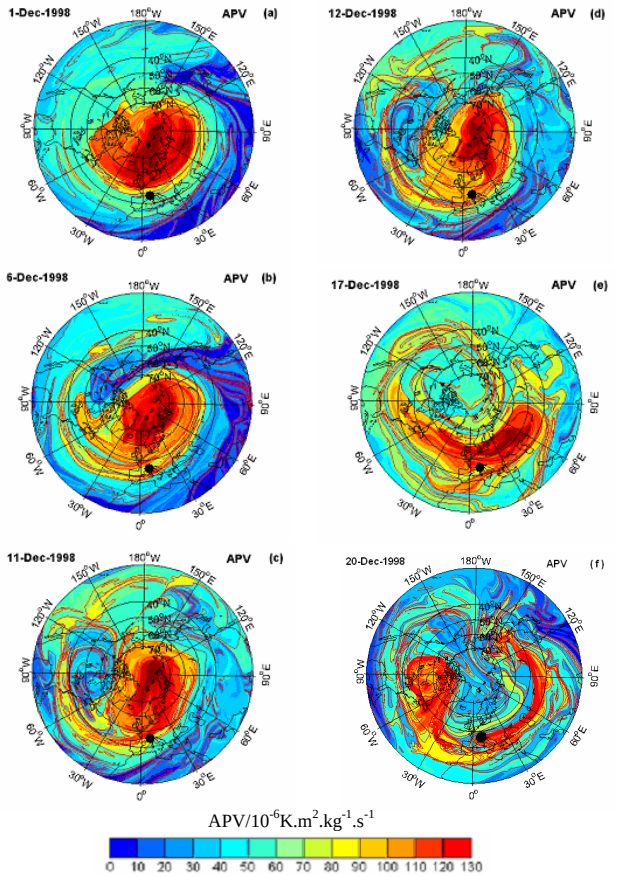

Fig. 8. North Polar stereographic maps of advected PV (APV) at 950 K provided by MIMOSA simulation driven by the ECMWF ERA40 reanalysis data for the selected days in December 1998. The outermost circle designates the Equator, and "•" indicates the location of OHP lidar site (44° N, 6° E).

ACPD
7, 15739–15779, 2007

EGU

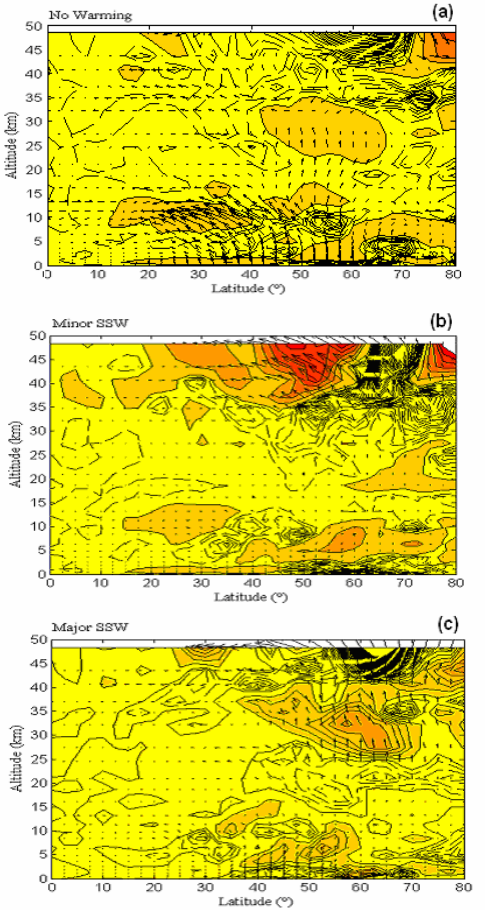

Fig. 9. Meridional cross section of Eliassen-Palm Flux and Zonal mean wind velocity. Contours represent div (F), in m.s-1 per day; Regions of easterly winds (negative values) are shaded **(a)** no warming (normal winter situation) **(b)** minor SSW on 6 December 1998 **(c)** major SSW 17 December 1998.

ACPD
7, 15739–15779, 2007

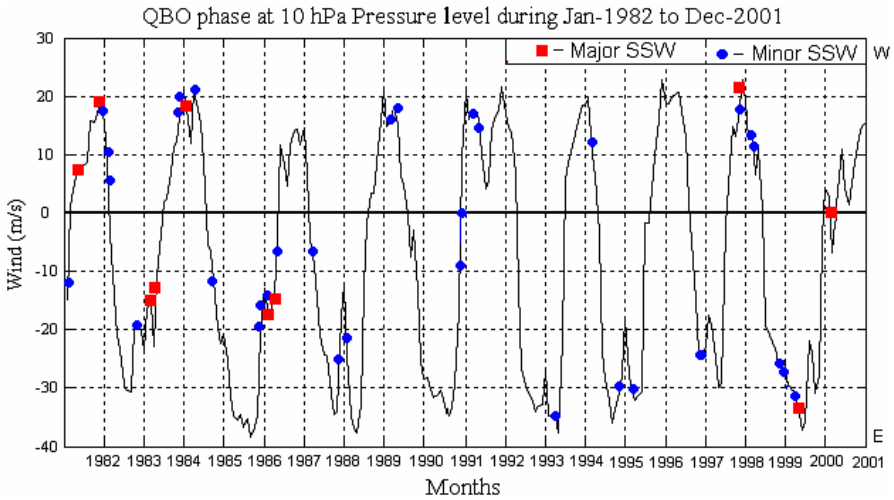

Fig. 10. QBO signature in monthly mean zonal wind obtained from a near equatorial region (Singapore; 1.30° N. 103.85° E); occurrence of major (red square marks) and minor (blue dots) warmings for the period from the year 1981 to 2001.

ACPD
7, 15739–15779, 2007

Atmos. Chem. Phys. Discuss., 7, 15739–15779, 2007
www.atmos-chem-phys-discuss.net/7/15739/2007/

Atmospheric Chemistry and Physics Discussions

20-year LiDAR observations of stratospheric sudden warming over a mid-latitude site, Observatoire de Haute Provence (OHP; 44° N, 6° E): case study and statistical characteristics

D. V. Charyulu[1,2], V. Sivakumar[3], H. Bencherif[1], G. Kirgis[1,4], A. Hauchecorne[4], P. Keckhut[4], and D. Narayana Rao[2]

[1]Laboratoire de l'Atmosphère et des Cyclones, UMR 8105 CNRS/Université/Météo-France, Université de LaRéunion, Messag 9 BP 1751, Saint Denis, Réunion Island, France
[2]National Atmosphere Research Laboratory, Tirupati, Andhra-Pradesh, India
[3]National Laser Centre, Council for Scientific and Industrial Research (CSIR), P.O. Box 395, Pretoria 0001, South Africa
[4]Service d'Aéronomie, IPSL, UMR CNRS, Paris, France

Received: 28 June 2007 – Accepted: 25 September 2007 – Published: 12 November 2007

Correspondence to: D. V. Charyulu (vidya@univ-reunion.fr)

Abstract

The present study delineates the characteristics of Stratospheric Sudden Warming (SSW) events observed over the Observatoire de Haute Provence (OHP: 44° N, 6° E). The study uses 20 years of Rayleigh LiDAR temperature measurements for the period, 1982–2001, which corresponds to 2629 daily temperature profiles. Characteristics of warming events, such as type of warming (major and minor), magnitude of warming, height of occurrence and day period of occurrence are presented with emphasis on wave propagation and isentropic transport conditions. The major and minor warming events are classified with respect to temperature increase and reversal in the zonal wind direction in the polar region using reanalysis data from the National Centre for Environmental Prediction (NCEP). SSWs occur with a mean frequency of 2.15 events per winter season. The percentage of occurrence of major and minor warming events are found to be ∼23% and ∼77%, respectively. The observed major and minor SSW is associated with a descent of the stratopause layer by −6 to 6 km range. The heights of occurrences of major SSWs are distributed between 38 km and 54 km with magnitudes in the 12.2–35.7 K temperature range, while minor SSW occurrences appear in the 42–54 km range, closer to the usual stratopause layer (∼47 km) and with a slightly larger range of temperature magnitude (10.2–32.8 K). The observed major and minor events are examined in connection with Quasi-Biennial Oscillation (QBO) phases.

1 Introduction

The middle atmosphere (which mainly covers stratosphere and mesosphere) is the region of the atmosphere from approximately 12 km to 80 km altitude. Studies of dynamic, radiative and chemical processes in this region have expanded greatly in recent years owing to impacts by human activities on the stratospheric ozone layer and the coupling between stratospheric changes and surface climate (McIntyre, 1982; Andrews et al., 1985).

It is well known that there is a large interannual temperature variation in the Northern Hemisphere winter stratosphere. The greatest variation is observed due to Stratospheric Sudden Warming (hereafter, referred as SSW) (Scherhag 1952; Labitzke, 1977, 1981, 1982; Schoeberl, 1978; Quiroz, 1986; Andrews et al., 1985) and so far, evidence shows that the occurrence of SSW, may have a marked influence on polar stratospheric temperatures (e.g., Matsuno, 1971; Andrews et al., 1985), troposphere circulation (e.g., Quiroz, 1977; O'Neill and Taylor, 1979; Baldwin and Dunkerton, 1999) Northern Hemisphere annular mode (NAM) and on zonal flow in the Upper Troposphere-Lower Stratosphere (UT-LS) region (e.g., Limpasuvan et al., 2004). Historically, SSW has been viewed as a large-scale dynamical meteorological phenomenon in the stratosphere. Observational, theoretical and modeling studies on SSW have expanded greatly in recent years in attempts to understand the stratospheric circulation and relate it to dynamical-chemical changes with emphasis on stratosphere ozone content.

Briefly, during some winters, the zonal-mean configuration is dramatically disrupted with polar stratospheric temperatures increasing rapidly with time, leading to a poleward increase of zonal-mean temperatures and on occasion, a reversal of zonal-mean winds to an easterly direction exists. Such an event is defined as Stratospheric Sudden Warming (SSW) (Andrews et al., 1985). It is a large-scale dynamic event with a QBO signature of occurrence (Baldwin et al., 2001) which could increase the temperatures near the pole by ∼40–60 K in one week. Major warmings may not occur every winter, but occur mostly in every alternative winter. Minor warmings do occur more frequently in every winter (e.g. Andrews et al., 1985; Dunkerton and Baldwin, 1991). Major warming occurs mostly during mid-winter in Northern Hemisphere, resulting in the strongest perturbations in zonal-mean temperature and zonal-mean wind reversal (westerly to easterly) (Lorenz, 1967; Dunkerton and Baldwin, 1991).

In addition, a SSW may either cause a polar vortex displacement from the pole or may split the vortex into two parts (often referred as SSW generated by wavenumber 1 and wavenumber 2). Some major warmings exhibit a hybrid character with the split

polar vortex being displaced asymmetrically from the pole. On the other hand, minor warmings occur every winter with weaker perturbations in zonal-mean temperature and no reversal of the zonal-mean wind. Furthermore, they do not lead to polar vortex displacement or vortex splitting. Final warmings occur at the end of the winter and they mark the transition between winter westerly winds and summer easterly winds which leads to polar vortex breakdown. Canadian warmings may occur in early winter (mid-November to early December) showing abrupt temperature increases similar to the major warmings. During Canadian warmings, the warm Aleutian High advects eastward with in a few days from its usual position over the dateline towards 90° W line of longitude over Canada. In this case, the polar vortex does not breakdown but distorts strongly and displaces from the pole (Andrews et al., 1985; Donfrancesco et al., 1996; Marenco et al., 1997; O'Neill, 2003).

The investigation of stratospheric warming has been greatly advanced in recent years, using conventional data retrieved from radiosondes, rocketsondes, falling spheres, ground based LiDAR and satellite data. In order to measure continuous short term changes in temperature over long periods of time and over a particular place, ground based LiDAR techniques are advantageous due to its good range and superior temporal and altitude resolution. Other techniques like satellites, which offer the temperature structure over the globe with good temporal coverage, are unable to provide the high altitude resolution. Rocketsondes and falling spheres offer relatively poor vertical resolution and accuracy due to uncertain radiative and aerodynamic heating corrections. Another advantage in LiDAR monitoring is that it is economical in comparison with other techniques. In fact, LiDAR may be operated continuously at different places during specific campaigns or routinely for long-term survey with limited financial and manpower resources (Labitzke and van Loon, 1999).

So far, many observational studies were carried out in order to characterize SSW events using temperature measurements from LiDAR, satellite and rockets over the Northern and Southern Hemispheres. Such warming events, based on temperature and zonal wind fields, have been individually classified as major, minor or Canadian

warmings. Most of these events are documented in the literature as case studies but few statistical results are available (e.g. Appu, 1984; Dunkerton and Delisi, 1986; Delisi and Dunkerton, 1988; Dunkerton et al., 1988).

The first SSW observation was reported by Scherhag in 1952, using radiosonde measurements over Berlin. Later, Schoeberl (1978) provided a review on the theory and observations of stratospheric warming using results reported from different places. The results suggested that the warming is confined to the Northern Hemisphere, especially during winter over polar region (Andrews et al., 1985). Similarly, there is also evidence of SSW occurrences in the Southern Hemisphere (e.g. Baldwin et al., 2003). The cause of SSWs is mainly attributed to planetary wave breaking (Hauchecorne and Chanin, 1983; Marenco et al., 1997) and gravity wave propagation (Whiteway and Carswell, 1994; Whiteway et al., 1997). There are many results reported as case studies for high latitude (Whiteway and Carswell, 1994; Donfrancesco et al., 1996; Whiteway et al., 1997; Duck et al., 1998; Walterscheid et al., 2000) and very rarely for mid- (Hauchecorne and Chanin, 1983) and low-latitudes (Sivakumar et al., 2004). The recent observation made by Sivakumar et al. (2004) recorded the first finding of a SSW over low latitudes and illustrated that the warming is due to an increase in planetary-wave activity. Their calculations on Eliassen-Palm (E-P) flux from ECMWF reanalysis, shows clear evidence of an equator-ward propagation of planetary waves consecutive to a major warming episode over polar region. The study evidenced that the SSW is not only focused towards high/mid latitudes, but that it can also extend to low latitudes depending on the strength of the warming. So far, most studies on SSW have been addressed at high latitude regions and for limited observational periods. Even then, there is no long database available to address such phenomenon for a extensive statistical study.

We use the 20 years of ground-based LiDAR data collected at the Observatoire de Haute Provence (OHP; 44° N, 6° E) from January 1982 to November 2001, to investigate SSW characteristics. OHP is a French observatory that acts as a primary NDACC (Network for the Detection of Atmosphere Composition Change) site. OHP

Rayleigh LiDAR has been operating regularly since 1979, and serves as a long-term dataset in studying and understanding the mid-latitude middle atmosphere thermal structure and dynamics (e.g. Hauchecorne and Chanin, 1980, 1983; Randel et al., 2002; Hauchecorne et al., 2002).

The present paper is structured as follows: Sect. 2 gives details about the datasets and analyses tools used to examine SSW events. In Sect. 3, we discuss the OHP observed LiDAR temperature evolution and calculations of climatological and seasonal mean profiles. Section 4 presents a case study on the winter-1998/1999 and introduces the criteria involved to identify and classify SSW events over OHP. Results and discussions on observed statistical characteristics of SSWs such as dates of occurrence, duration of occurrences, magnitude of warm temperature, descent height of stratopause, occurrence of SSW according to the state of QBO and agreement of date of occurrence of SSWs with previous reports are presented in Sect. 5.

2 Data and analysis

2.1 Daily temperature profiles

2.1.1 LiDAR profiles

A LiDAR dataset refers to a night time temperature profile measured by a ground based Rayleigh LiDAR system located at the Observatoire de Haute Provence (OHP; 44° N; 6° E), south of France. Temperature profiles are retrieved from the back-scattered photons in each successive atmospheric layer. The back-scattered photons provide the vertical profile of relative atmospheric density. Assuming that the atmosphere is in hydrostatic equilibrium, a pressure profile can be computed by combining a reference atmospheric model and a measured density profile along the studied height range (typically 30–80 km) with a height resolution of 300 m (Hauchecorne and Chanin, 1980; Chanin and Hauchecorne, 1984). Adopting the perfect gas law and using the derived

density and pressure profiles, the temperature profile can be deduced by following the retrieval method developed by Hauchecorne and Chanin (1980).

A 20-year LiDAR dataset covering the period from 1 January 1982 to 6 November 2001 is used to examine the middle atmosphere thermal structures to detect SSW events over OHP. The total number of observations correspond to 2629 and are distributed almost evenly in each month. The monthly distribution of LiDAR observations is presented in terms of a histogram in the Fig. 1. It illustrates an average number of observations of ∼225 profiles per month. In order to examine the seasonal characteristics of temperature over OHP, the 2629-daily LiDAR profiles are grouped into each three months in the following manner;

- 749 records during winter (December–January–February: DJF),
- 580 records during spring (March–April–May: MAM),
- 639 records during summer (June–July–August: JJA), and
- 661 records during autumn (September–October–November: SON).

Based on earlier reported results, SSW events occur only during winter and nearby periods. This leads us to enlarge the winter period by including the early and late winter LiDAR records: the enlarged winter is from November to March and it is made of 1233 temperature profiles (i.e. ∼47% of the complete LiDAR datasets).

Besides the above LiDAR observations, additional datasets are required to classify and interpret the noticed SSW events. The following sub-sections give a brief description of UARS/HALOE, NCEP, ECMWF-ERA40 datasets and of the high-resolution MIMOSA model.

2.1.2 UARS/HALOE profiles

Halogen Occultation Experiment (HALOE) is on board the Upper Atmosphere Research Satellite (UARS) launched on 12 September 1991. It uses solar occultation

method to measure vertical profiles of Ozone (O_3), Hydrogen Chloride (HCl), Hydrogen Fluoride (HF), Methane (CH_4), Water Vapor (H_2O), Nitric Oxide (NO), Nitrogen Dioxide (NO_2), Temperature and Aerosol Extinction at 4 infrared wavelengths. It uses the atmospheric transmission measurements in the 2.8-μm CO_2 and for the retrieval of temperature profiles. The temperature data obtained after the removal of aerosol contamination (Net-ASCII, Version 19). Further detailed descriptions of HALOE satellite data are available on the web (http://haloedata.larc.nasa.gov/home/index.php). Information about validation and accuracy of HALOE data can be found in published papers: Russel et al. (1993); Hervig et al. (1996); Sivakumar et al. (2003, 2004).

In the present study, quasi-simultaneous measurements (same date as LiDAR measurements) of UARS/HALOE (sunrise and sunset) overpasses over OHP (44° N, 6° E) site, within ±5° in latitude and ±10° in longitude ranges from winter 1991/1992 to winter 2001/2002 are examined.

3 Meteorological data

3.1 NCEP data

The National Center for Environmental Prediction (NCEP) provides daily meteorological data on a 2.5°×2.5° horizontal grid for 17 pressure levels: between 1000- and 10-hPa (Kalnay et al., 1996). Earlier reports suggest that the North Pole NCEP temperatures in winter, particularly in February and March, during 1979–2001, are in very good agreement with FU-Berlin data and ECMWF-ERA40 reanalysis datasets (Labitzke and Kunze, 2005). NCEP/NCAR reanalysis data is archived on the NOAA Climate Diagnostics Center web page (http://www.cdc.noaa.gov/). In the present study, we use a NCEP zonal mean temperature at 80° N and zonal mean wind at 60° N at the 50-, 30-, and 10-hPa pressure levels to examine temperature and wind conditions over the pole.

3.1.1 ECMWF-ERA40 re-analysis data

Information about prevailing meteorological and dynamical conditions in the northern stratosphere is addressed using ERA40 re-analyses. The latter is archived on the ECMWF (European Centre for Medium-Range Weather Forecasts) website, http://www.ecmwf.int/research/era/. Indeed, ECMWF-ERA40 horizontal winds and temperature fields are extracted on a 2.5°×2.5° grid from 1000- to 1-hPa pressure levels. The extracted data is used in the present study to derive the Ertel's Potential Vorticity (EPV) and Eliassen-Palm (E-P) flux.

4 Dynamics/transport analysis tools

4.1 EPV contour advection by MIMOSA model

MIMOSA (Modélisation Isentrope du transport Mésoéchelle de l'Ozone Stratosphérique par Advection) is a high-resolution advection contour model of the Ertel's Potential Vorticity (EPV). It was developed at the Service d'Aéronomie, a French CNRS research unit, by Hauchecorne et al. (2002). The model can be used both to reproduce global atmosphere dynamical events and small-scale events and especially to interpret the events such as ozone or aerosol laminae (Bencherif et al., 2003; Morel et al., 2005; Semane et al., 2006). The model starts from the ECMWF PV field interpolated on the MIMOSA orthogonal grid. The PV of each grid-point is advected using ECMWF winds. The model runs on an isentropic surface and two domains centred at the North and South poles with a resolution of 3 points grid per degree. The fields produced for each hemisphere are then linked together within a latitude band of 5° width, centred over the equator. A full description of the MIMOSA model is given in Hauchecorne et al. (2002).

In the present study, the MIMOSA model is run in order to construct Advected Potential Vorticity (APV) maps on stratospheric isentropic levels.

4.2 Eliassen-Palm flux

In order to gain insights into the dynamical processes occurring during SSW events and in particular to study the planetary wave drive and breaking, the Eliassen-Palm (E-P) flux vector (F) and its divergence (∇F) are used. It is defined by the following equations (Andrews et al., 1987):

$$F = \left\{f_{(\phi)}, F_{(z)}\right\} = \left\{-\rho_0 a \cos\phi \left(\overline{v'u'}\right), f\rho_0 a \cos\phi \left(\frac{\overline{v'\theta'}}{\overline{\theta'}}\right)\right\} \text{ and}$$

$$\nabla.F = \frac{1}{a\cos\phi}\left(F_\phi \cos\phi\right)_\phi + \left(F_{(z)}\right)_z \quad (1)$$

The over-bars denote zonal means and primes denote the deviations with their respective means. The other symbols have usual meanings. Further explanations may be found in Andrews et al. (1987).

During winter, Planetary Waves (PW) generally propagates from the troposphere to the stratosphere and towards the equator (Eliassen and Palm, 1961; Kanzawa et al., 1984). These waves highly disturb the middle atmosphere temperature and act as one of the generative mechanism for the occurrence of SSW. The orientation of E-P flux vectors indicates the direction of Planetary Wave propagation (Dunkerton and Delisi, 1986; Delisi and Dunkerton, 1988) and the convergence of the E-P vectors ($\nabla.F<0$) indicate the Planetary Wave (PW) breaking.

5 Seasonal variability of temperature

This section aims to illustrate the general temperature behavior and the seasonal mean temperature profiles as derived from OHP LiDAR observations. The time evolution, recorded by LiDAR, of temperature, for the 30–70 km altitude range is depicted in Fig. 2. The blank spaces in the figure correspond to the actual data gap.

In order to underline the climatological thermal structure and corresponding variability in terms of seasonal variation of mean temperatures and respective standard deviations, the winter, spring, summer and autumn mean temperature profiles are obtained as follows; daily temperature profiles of the months of December–January–February (winter), March–April–May (spring), June–July–August (summer) and September–October–November (autumn) data are grouped irrespective of the year (from 1982 to 2001) and averaged to obtain one value per day and per kilometer. Similarly, enlarged winter/summer mean profiles are calculated by taking into account early and late winter/summer months (i.e. enlarged winter: November to March; enlarged summer: May to September). The obtained seasonal profiles are presented in the Fig. 3. The overall temperature profile, obtained by averaging the 20-year dataset irrespective of month and year, is superimposed (with start symbols). It shows a maximum temperature of ∼264.5 K and a stratopause height at ∼47 km. The observed stratosphere – lower mesosphere region is warmer during summer and cooler during winter. The summer stratopause is found at ∼47.5 km with a maximum temperature of ∼268 K. The winter stratopause is found to occur at ∼45.5 km with a maximum temperature of ∼262 K, which is used as a reference value in the present study to calculate the descent of stratopause and the magnitude of the warm temperature respectively. At the stratopause height, the minimum temperatures are observed in the beginning of November and the maximum temperatures are observed in May–June period (figure not shown). This is in agreement with previous climatological studies for OHP site (Hauchecorne et al., 1991; Hauchecorne and Chanin, 1983; Leblanc et al., 1998; Sivakumar et al., 2006).

From seasonal temperature profiles (Fig. 3), one can see that spring and summer profiles exhibit a similar behavior at the stratopause region in terms of height (stratopause at ∼47.5 km) and temperature (∼268 K). The maximum descent of stratopause is obtained during winter (∼45.5 km). Note that by January the stratopause is found (figure not shown) at its lowest height (∼45 km). The enlarged winter (NDJFM) and summer (MJJAS) profiles and the respective standard deviations are presented in

Fig. 4 (a and b). For ease of comparison, the figure is superimposed by the 20-year over-all temperature profile. As expected, it is evidenced from the figure that winter deviations (±12 K) are approximately four times larger than summer deviations (±3 K) at usual stratopause level. This is consistent with wave disturbances increasing in the winter hemisphere. In fact, the winter stratosphere is disrupted mainly by gravity and planetary wave activity. These waves are generated mainly in the troposphere and in winter, they propagate with the westerly winds through the middle atmosphere.

6 SSW: A case study

6.1 SSW detection and classification criteria

A stratospheric sudden warming event is classified as major, minor, Canadian or final warming (e.g., O'Neill, 2003). The final warming characteristics are similar to the major warming, except that it occurs mostly during the end of winter. Both the major and final warmings lead to a breakdown of the cyclonic polar vortex. Therefore, in the present study, we classify the final warming as a major warming. Further, a warming is said to be Canadian when it occurs over Aleutian High region (Canada), (e.g., Labitzke and van Loon, 1999; O'Neill, 2003). Here, we classified the observed warming events into either minor or major warmings. In this regard, daily profiles are compared to the extended winter (NDJFM) mean profile.

When a temperature profile is 10-K (or 2σ) warmer than the enlarged-winter mean profile, we examine the zonal parameters in the polar stratosphere (using NCEP data at the 10-hPa pressure level), i.e., temperature and wind components at 80° N and 60° N respectively. A warming event is detected if the temperature evolution over polar region illustrates a significant increase. Further, if the warming is coincident with a zonal wind reversal (i.e., it becomes easterly), the warming is classified as a major one; otherwise it is classified as a minor.

6.1.1 Case study

As a case study, we investigate the SSW events observed during winter (NDJFM) 1998/1999. The corresponding temporal evolution of lidar temperature profiles from 1 November 1998 to 31 March 1999 is presented in the Fig. 5. During the above-said period, there are occurrences of missing LiDAR data (blank spaces). The figure illustrates the warm temperature in the stratopause height region. It is observed that on a few occasions, the values are greater than 280 K. However, on Fig. 4a, one can see that the stratopause is as high as ∼47 km with a maximum temperature of ∼261 K.

Taking into account temperature differences between LiDAR daily profiles and the enlarged-winter profile (sometimes more than +20 K), one can underline that the observed stratosphere was under several and successive warmings during winter 1998/1999. For illustration purposes, daily profiles corresponding to two successive warming episodes (i.e., 4–8 and 16–19 December) are shown in Fig. 7 (a and b), together with the over-all and the enlarged-winter profiles. Those two warming episodes do not exhibit similar temperature characteristics. However, it is observed that both of them are consistent with the quasi-simultaneous HALOE temperature profiles (derived from UARS/HALOE overpasses nearby OHP location at ±5° in latitude and ±10° in longitude).

By combining LiDAR observations and NCEP reanalysis, this case study section aims to focus on detection of warming events that occurred during the 1998/1999 winter over a mid-latitude site (OHP), following the detection criteria explained above.

- Early-December, Early January and Mid January > minor warming occasion and
- Mid-December > major warming occasion,

The noticed SSW temperature profiles for the above four occasions correspond during 4 to 8 December 1998, 16 to 19 December 1998, 5 to 9 January 1999 and 13 to 14 January 1999. To compare and classify the above said four SSW events into Major or Minor warmings, the NCEP data of zonal-mean temperature at 80° N and zonal mean

wind at 60° N at three different pressure levels (50, 30 and 10 hPa) are presented for the period from November 1998 to March 1999 in Fig. 6. The zonal mean temperature and wind at three different pressure levels follow each other. For classifying the events into a major/minor category, we have used only the temperature/wind information for the pressure levels at 10 hPa. Among the temperature profiles of the first SSW event from 4 to 8 December 1998, the warmest temperature profile is observed on 6 December 1998. The warm stratopause located at 46 km (see Fig. 7a) is in good agreement to compare the temperatures at 10 hPa (about 30 km) pressure level observed on the same day by NCEP (see Fig. 6). However, no zonal mean wind reversal is observed (in NCEP data) for the same day or few days before to the 6 December 1998. Therefore, the SSW event noticed on 6 December 1998 is classified as minor warming. Whereas, during the second SSW event from 16 to 19 December 1998, the maximum temperature is observed on 17 December 1998 and, is again, in good agreement for comparison with the NCEP observations. The peak in the NCEP temperature is noticed on the same day (see Fig. 6) and zonal mean wind reversal is also observed (in NCEP data) on the same occasion. Therefore, this SSW event, on 17 December 1998, is classified as major warming. Similarly, the third SSW event occasion from 5 to 9 January 1999, the warmest day temperature profile is observed on 7 January 1999, which is in agreement after comparing the peak temperature observed on the same day by NCEP at 10 hPa (Fig. 6). No zonal mean wind reversal is observed (in NCEP data) a few days before to the 7 January 1999, so, the SSW event noticed on 5 January 1999 is classified as minor warming. The fourth SSW event recorded warm temperatures observed on the 13 and 14 January 1999. The warmer day temperature profile observed on 14 January 1999 is in good agreement to compare the temperatures observed on the same day by NCEP (Fig. 6). In the same period, no zonal mean wind reversal is noticed in the NCEP data sets and therefore this event (14 January 1999) is classified as minor warming. The time gap in the occurrence between these four SSW events is 11 days, 20 days and 7 days. Warm temperature of 15.1 K, 28.7 K, 18.1 K and 14.4 K is noticed on the above four SSWs (6 December 1998 (minor), 17 December

1998 (major), 7 January 1999 (minor), and 14 January 1999 (minor)) respectively. Descent of stratopause occurred at ∼1 km, ∼6 km, ∼2 km and ∼3 km respectively. All of the four above mentioned SSWs have occurred when the QBO was in the west phase.

Among the above noticed four SSW events, we have chosen the first (6 December 1998 – Minor SSW) and second (17 December 1998 – Major SSW) events to illustrate the method of analysis. Figure 7a and b shows daily profiles of temperatures observed from 4 to 8 December 1998 and from 16 to 19 December 1998 using LiDAR. These two SSW event occasions are also noticed in NCEP data winter 1998–1999 as depicted in Fig. 6.

In Fig. 7a, the HALOE measured temperature profile on 6 December 2006 closely follows the OHP LiDAR observed profile on 5 December 2006 and is comparable with the OHP LiDAR measured temperature on 6 December 2006 with a 2 K degree difference in temperature. In Fig. 7b, the HALOE measured temperature profile on 17 December 1998 is 6 K cooler and closely follows the general trend of the OHP LiDAR measured temperature profile on the same day. The slight difference in magnitude of temperature between OHP LiDAR profile and HALOE profile might be due to the time difference of LiDAR (refer to night time) measurements due to the passage of HALOE satellite (refer to sunset) over OHP.

7 Associated planetary wave activity and large scale transport

7.1 Advection of potential vorticity

To study the atmosphere dynamic related process (say, PW) during the sudden stratospheric warming events, we use isentropic maps of Ertel's Potential Vorticity (EPV). This approach has been followed elsewhere and is used to study SSW in connection with the breaking of planetary waves (e.g. McIntyre and Palmer, 1983; Dunkerton and Delisi, 1986). Their hypothesis suggests that large-scale wave breaking leads to polar-vortex distortion and erosion, and may induce stratospheric warming. Hypothe-

ses made by Dunkerton and Delisi (1986) suggested that the temporal evolution of the size, shape and orientation of the main circumpolar vortex, is clearly revealed by the potential vorticity field. The size of the vortex determines the range of latitudes over which planetary and Rossby waves are able to propagate.

Figure 8a–f shows north polar stereographic projection maps of advected PV (APV) evaluated on the 950-K isentropic surface. These maps were provided by the MIMOSA simulation which were driven by ECMWF-ERA40 reanalysis data for the days 1, 6, 11, 12, 17 and 20 December 1998. The inner and outermost circles designate the 70° N and the Equator respectively. The OHP lidar site is indicated by the symbol "•". Contours of APV values give a well-defined picture of APV gradients and large-scale structures.

The APV map obtained for 1 December 1998 (Fig. 8a) shows a relatively more symmetric and undisturbed vortex over the polar region. Incursion of low-PV values (tropical air-masses) in the shape of a tongue can be seen (see Fig. 8a) over the region with a longitudinal extension from 105° E to 135° E. By 6 December 1998 (during minor SSW event) the incursion of a low-PV caused further extension westward up to 90° W, while high-PV values (polar/vortex air-masses) have tilted and drifted southward over the mid- and subtropical-latitudes, including the OHP location. The spread of the polar air-masses continued on the following days in the form of filamentary structures pulled over in the equator-ward direction. These structures then mixed-up with tropical air-masses, as illustrated by Fig. 8c, d. On 17 December 1998 the polar air-masses almost shifted from high- to mid-latitudes (see Fig. 8e), presumably as a result of the major warming occurrence. On the following days, the high-PV air masses moved further southward and scattered over the mid-latitudes in a shape of a very-large-belt surrounding the low-PV air-masses over polar region (see Fig. 8f).

From a comparison between the minor warming (4–8 December) and the major warming (16–19 December), one observes a significant differences in shape, extent and orientation of the polar vortex. In fact, during the minor warming, the polar vortex keeps relatively symmetric and high-PV air-masses remain located over high-latitude

regions (see Fig. 8b). In contrast, during the major warming, before splitting, the polar vortex is asymmetrically displaced equator-ward and materials are pulled out-off the polar region in the form of filamentary structures as far as tropics/subtropics. This is in good agreement with the arguments concerning the distinction of potential vorticity evolution between major and minor warmings given by McIntyre (1982).

7.2 Planetary wave trajectories: E-P flux

Eliassen-Palm (E-P) flux is used to interpret Planetary Waves (PWs) in terms of propagation and trajectory in the meridional plane. For the present study, wave fluxes in the E-P vector's formulation are calculated using ECMWF ERA-40 reanalysis data. For a clear visualization throughout the stratosphere, the E-P vectors are multiplied by the factor $e^{z/H}$ (Mechoso et al., 1985) and $F_{(Z)}$ is magnified by factor 150 with respect to $F_{(\phi)}$ (Randel et al., 1987). Figure 9 is superimposed on the plot of wave driving (contours), which is proportional to the E-P flux divergence; $D = \frac{1}{\rho_0 a \cos\phi} \nabla . F$.

The Fig. 9a–c shows the meridional cross section of the directions of E-P flux vectors (arrows), calculated for normal winter conditions (no warming day), minor SSW (6 December 1998) and major SSW (17 December 1998). The direction of E-P flux, indicates the active vertical propagation of the wave flux, for planetary waves propagating from one height and latitude to another. During a normal winter (see Fig. 9a), one notices that the E-P arrows in the low latitude upper troposphere have strong equatorward components. The length of E-P arrows in the stratosphere is small, indicating that the values are less. Figure 9b, c shows E-P cross-section for the days of minor and major SSWs observed on 6 and 17 December 1998. On 6 December 1998, strong upward and equatorward movement appeared in the mid-latitude, upper stratosphere region and the length of E-P flux values are higher than those on the day of no warming (see Fig. 9a). On 17 December 1998, one can see strong upward movement in the mid-latitude, upper stratosphere as well as in the lower stratosphere. While a positive $\nabla * \bullet E$ region in the middle latitude troposphere, indicates the source of momentum in

that region.

It is evident from the figure, that the OHP LiDAR has observed minor and major warmings (see Fig. 6b and c) over OHP (44° N) that occurred at ∼46 km and ∼40 km respectively. It is well interpreted by the E-P flux analysis, in Fig. 9b and c, that for minor and major warmings over 44° N region, the "focusing" of the waves is mostly around 40 km and 35 km respectively. On 6 December, the day of the minor warming over OHP, the wave propagation is towards the equator and tropical region which differs from the situation on major warming day, where the wave propagation mostly "focuses" over mid-latitude region.

It is interesting to see the strong E-P flux which exists on the day of minor warming. The direction of E-P flux is equator-ward and towards the tropical region, where the stronger wave activity and convergence of E-P flux are likely to produce rapid deceleration of zonal-mean zonal wind and the associated increase in temperature. It can be interpreted that this situation might have lead to a major warming (e.g. McIntyre 1982). On 17 December, the day of major warming, the "focusing" of the waves, at around 30 km to 35 km over 44° N latitude region, and the zonal mean wind reversal (shaded and contours) exists exactly over the region where the OHP is located. On 25 December 1998, as an example for a "no warming" day (Fig. 9a), the middle atmosphere returns to normal, with planetary-wave activity remarkably weaker in the stratosphere region.

8 SSW: Statistical characteristics

8.1 SSW general characteristics

Twenty years of night-time quasi-continuous Rayleigh LiDAR temperature data is used to obtain the statistical characteristics of SSW events that were observed over OHP. The characteristics, listed in the Table 1, are provided in terms of dates of occurrence, descent of stratopause, magnitude of temperatures, types of warming (major/minor)

and occurrence of SSWs in relation with the phase of QBO. The following are the main salient features obtained from the statistical study;

- There are 43 SSW events recorded in winter months (NDJFM). Among 43 SSW events, 10 events are major warmings and 33 events are minor warmings.
- Among 10 major warmings, 4 major warmings are followed by minor warmings and 2 are preceded by minor warmings during the yearly winter (NDJFM) period.
- Among 43 events, the number of occurrences of SSWs are 2, 15, 12, 8 and 6, respectively in November, December, January, February and March. Out of 10 major events, none were observed in November, 2 events observed in December and January respectively, 3 events observed in February and March repsectively. Similarly, the 33 minor events are distributed as follows: 2, 13, 10, 5 and 3 in November, December, January, February and March repsectively.
- The decent of stratopause with respect to winter mean stratopause height, was varied from 1 km to 6 km, for major warmings and from 0 km to 6 km in the case of minor warmings. The mean decent of height is ∼1.2 km for major warming and ∼5.3 km for minor warming.
- The magnitude of warmings with respect to the overall winter temperature profile, varied from 12.2 K to 35.7 K for major warmings and from 10.2 K to 32.8 K in the case of minor warmings. On average, the magnitude of the warm temperature is noted as ∼20.1 K for major warming and ∼18.8 K for minor warming.

9 Distribution of SSWs in relation with QBO phase

Although the QBO is a tropical phenomenon, it affects the stratospheric flow from pole to pole (Baldwin et al., 2001) and it dominates the zonal wind in the tropical stratosphere (e.g., Naujokat, 1986). Thereafter, a suggestion was made by McIntyre (1982)

that deep equatorial easterlies may favor the occurrence of a strong mid-winter warming and that SSWs tend to occur more frequently during the easterly phase of the equatorial QBO than the westerly phase (Labitzke, 1982). Dunkerton (1988) studied the occurrence of major SSWs in relation to QBO by using 35 years of satellite data. Their study suggested that Northern Hemisphere winter major SSWs have not occurred when the equatorial monthly mean zonal winds are deep westerly. And more than half of the major SSWs have occurred when the equatorial flow is easterly at 10 and 50 hpa levels. In order to study the apparent connection between the QBO and SSW, particularly to study the distribution of major or minor warming in relation with QBO phase and in future to determine how much a particular warming contributes to interannual variability, we use the QBO data documented by Naujokat (1986), which is developed by using monthly averages of rawinsonde observations at Singapore (1° N, 103° E), as well as two other stations (Canton Island (2.46° S, 171.43° W), Gan/Maledives (0.41° S, 73.09° E)) for earlier years. They are available at 10, 15, 20, 30, 40, 50 and 70 hPa.

Using the above 20 years of SSW statistics (see Table 1) and the monthly mean zonal wind at a 10 hPa pressure level (see Fig. 10), the frequency of occurrence of major and minor warming in relation to QBO phase is summarized as follows;

- Among a total of 43 SSW events, 23 events are observed when QBO is in east phase, 18 events are observed when QBO is in west phase and remaining 2 events are observed when the QBO is in the transitional phase between east/west or west/east.
- Among 10 major SSW events, 5 events are observed when the QBO is in east phase, 4 events are observed when the QBO phase is in west phase and 1 event is observed in the transitional phase.
- Among 33 minor SSW events, 18 events are observed when the QBO is in east phase, 14 events are observed when the QBO phase is west and 1 event is observed when the QBO is in the transitional phase.

– When the QBO phase is west, maximum warm temperature and maximum descent of stratopause is observed as 28.8 K and ∼6 km respectively; whereas when QBO phase is east, the maximum warm temperature and maximum descent of stratopause observed is 35.7 K and ∼6 km respectively.

Table 1 presents the statistical characteristics of SSWs which were observed over a mid-latitude site in the Northern Hemisphere (OHP). The SSWs occurred in 20 sequential winter seasons (November to March) and their classifications are presented. With the objective of classifying them into major and minor warmings, the correlation of occurrence between the onset dates of warming events in the NCEP and OHP data sets, to the dates of occurrence of SSW events noticed in OHP LiDAR data is observed. Only the nearest available dates of onset of circulation reversal (westerly to easterly) is noticed in the NCEP data (zonal mean temperature at 80° N and zonal mean wind at 60° N at 10-hPa pressure level) and are presented in the first column of Table 1. Note that the onset dates of circulation reversal observed in NCEP data during winters 1990/1991, 1992/1993 and 1996/1997 are not presented in the first column of Table 1. In the second column, we report the dates of occurrence of 42 SSW events, during the above mentioned period noticed in the OHP LiDAR data, and their classification using the usual criteria (see Sect. 4a) as either a major (M) or minor (m) SSW event. In the second column, the "+" sign or "−" sign is together displayed with either an "M" or "m" which denotes the phase state of QBO ("+" denotes west and "−" denotes east phase) during a major (M) or minor (m) warming event. In columns 3 to 6, the statistical characteristics of noticed SSWs, such as magnitude of warm temperature (ΔT), warm stratopause height, mean winter stratopause height and descent of stratopause, in OHP lidar data, are presented respectively. In the winter of 1981/1982 (using lidar data since 1 January 1982), two SSW events are noticed; the first one occurred on 2 February 1982 and the second on 31 March 1982. Figures 2 and 4 of Hauchecorne and Chanin (1983) shows a "strong minor warming" that has commenced on 2 February (earliest date of onset) over OHP, which has been classified as a minor warming event. The event observed on 31 March 1982 was not reported by Hauchecorne and

Chanin (1983), even though a NCEP observation is made earlier. Based on Naujokat and Labitzke (1993), we have classified this event as a major warming. In winter 1982/1983, four warming occasions were noticed at the end of December and at the end of January. Among the four occasions, based on circulation reversal observed on 17 December 1982 in NCEP data, the event observed on 22 December 1982 is classified as a major warming and the remaining three events were classified as minor warmings. In winter 1983/1984, among the three warming events observed in the early winter, end of February and beginning of March, the events noticed on 9 November and 4 March (based on NCEP observation) were classified as minor and major warmings respectively. In the case of event observed on 23 February, the NCEP observations show circulation reversal one day later to the SSW observed over OHP and based on Naujokat and Labitzke (1993), the event is therefore classified as a major SSW. In winter 1984/1985, four warming events were noticed in the beginning of December, beginning of January and in the middle of March. Based on NCEP observations till the end of December, the events observed on 4 and 11 of December were classified as minor warmings, but the event observed (over OHP) on 4 December was reported as a Canadian warming for the same day by Naujokat and Labitzke (1993). The event observed on 1 January is also reported by them as major mid winter warming. Based on NCEP observations, it is classified as major warming. The event observed on 14 March was reported as a final warming by them. Based on NCEP observations during February and March, it is classified as a minor warming. During winter 1985/1986, no circulation reversal was observed in NCEP data, hence the event noticed on 27 November is classified as a minor warming. In winter 1986/1987, six warming events were observed during December, January, end of February and the end of March. Based on zonal wind circulation reversal in NCEP data observed from 23 to 27 January and 21 to 24 February, the events of 1 and 23 December, 4 January and 24 March events were classified as minor warmings and the events observed on 23 January (Manney et al., 2005) and 27 February has been classified as major warmings. All events observed during winter 1987/1988 to 1997/1998 were classified as minor warmings based on the

fact that no wind reversal was observed in the NCEP data. In winter 1998/1999, four events were observed in December and January and based on NCEP observations of wind reversal noticed on 15 to 21 December, the event observed on 17 December is classified as major warming. The same event was reported by Manney et al. (1999) for the day of 15 December. The remaining events of 6 December, 7 and 14 January were classified as minor warming. In winter 1999/2000, four warming events were found during the end of December, beginning of February and the end of March based on the onset of wind reversal observed in NCEP data on 21 March. Among the events of 22 and 30 December, 4 February and 27 March, the event observed on 27 March was classified as a major warming and the remaining three events were classified as minor warmings. In winter 2000/2001, one event was observed on 15 February (Jacobi et al., 2003) and was classified as a major warming based on the circulation reversal observed on 12 to 23 February in NCEP data.

The magnitude of maximum temperature is observed in the order of 270–280 K over the stratopause region at 40 to 60 km. The magnitude of maximum warm temperature observed over OHP (mid-latitude station) is 35.7 K, which is comparable with the warm temperatures observed, thus far, over mid- and high-latitude stations (about 30 K) (Hauchecorne and Chanin, 1983; Whiteway and Carswell, 1994; Whiteway et al., 1997; Duck et al., 1998). Using EP flux calculations from ECMWF ERA 40 data, it was found that the SSW was mainly due to PW propagation from high to mid latitudes, consecutive to the warming episode over pole.

10 Conclusions

This paper reports the statistical characteristics of SSWs observed over a mid-latitude station (OHP, South of France) for the first time using 20 years (starting from 1 January 1982 to 6 November 2001) of Quasi-continuous LiDAR nighttime temperature data. Statistically, most of the OHP observed events, are in good agreement with the NCEP, ECMWF-ERA 40 and HALOE data sets. There are a few exceptions observed in the

SSW data sets when compared with the NCEP data. Here, it was noticed that some events occur a day earlier to the events observed in the other (OHP, ECMWF and HALOE) data sets.

SSWs occur with a mean frequency of 2.15 events per winter season. Out of 20 sequential winters starting from winter 1981/1982 to 2000/2001, 8 winters have had occurrences of major warmings and 17 winters have had occurrences of minor warmings. In total, 43 warming events have been identified. Among them, 10 events (about ∼23%) are major warmings and 33 events (about ∼77%) are minor warmings. The maximum-minimum magnitude of the warm temperatures, observed for the major and minor warmings, are in the range of 35.7–12.2 K and 32.8–10.2 K respectively. Also associated with major and minor warmings, the descent of stratopause layer by −4 to 6 km and −6 to 6 km respectively, is observed.

As a case study on winter 1998/1999, using the MIMOSA simulated APV evolution (Hauchecorne et al., 2002) and EP flux calculations based on ECMWF reanalysis, we found that the minor and major warming episodes are mainly attributed to the transport of tropical/polar air masses from high- and mid- to low-latitudes caused by Planetary Waves as a consecutive to the major warming episode over the polar region.

Among the total of 43 SSW events, 23 have occurred when the QBO phase was east and 18 have occurred when QBO phase was west. The remaining 2 events occurred when the QBO was in the transitional phase (east/west).

In the case of major warmings, the maximum magnitude of warm temperature was observed when the QBO phase was east, but in the case of minor warming the maximum magnitude of warm temperature was observed when the QBO phase was west. The minimum magnitude of warm temperatures observed for the both major and minor warmings is when the QBO phase was east. The quasi-periodic behavior of temperature with variations of 2 to 3 year periods is probably associated with the QBO.

However, the maximum warm temperatures for the both the major and minor warmings are observed when the QBO phase was east. Since the main objective of this present paper is to report the observed statistical characteristics of SSW, we briefly

discuss the dynamical process during the SSW occurrence in Sect. 4b (i) and (ii).

Finally, a table of observed statistical characteristics of SSWs is compiled. These benchmarks maybe used in future to contribute to modelling studies and to study the expected features of planetary wave propagation during SSWs. Further, we are interested in using primarily ground based LiDAR data in the Northern and Southern hemispheres to study and define the characteristics of SSW events which are observed at different low and mid-latitudes.

Acknowledgements. The Laboratoire de l'Atmosphère et des Cyclones (LACy) is supported by the French Centre National de la Recherche Scientifique (CNRS)/Institut National des Sciences de l'Univers (INSU) and the Conseil Régional de la Réunion. The authors wish to thank NOAA Climate Diagnostics Center (http://www.cdc.noaa.gov/) for providing portions of the NCEP data. The authors would like to thank the Goddard Space Flight Center, for providing HALOE satellite data through their web site http://haloedata.larc.nasa.gov/home/index.php. The authors are thankful to the European Centre for Medium-Range Weather Forecasts for providing portions of ECMWF-ERA40 reanalysis data through their web (http://www.ecmwf.int/research/era/). One of the authors, D. V. Acharyulu, acknowledges the Conseil Régional de la Réunion for financial support under the PhD fellowship scheme. The authors are thankful to A. Sharma for reading the manuscript and improving the readability.

References

Andrews, D. G., Holton, J. R., and Leovy, C. B.: Middle Atmosphere Dynamics, Academic Press, 1985.

Appu, K. S.: On Perturbation in the Thermal structure of tropical Stratosphere and Mesosphere in Winter, Indian J. Radio Space, 13, 35–41, 1984.

Baldwin, M. P. and Dunkerton, T. J.: The stratospheric major warming of early December 1987, J. Atmos. Sci., 46, 2863–2884, 1989.

Baldwin, M. P. and Dunkerton, T. J.: Downward propagation of the Arctic Oscillation from the stratosphere to the troposphere, J. Geophys. Res., 104, 937–946, 1999.

Baldwin, M., Gray, L. J., and Dunkerton, T. J.: The Quasi-Biennial Oscillation, Rev. Geophys., 39, 179–229, 2001.

Baldwin, M. P., Hirooka, T., O'Neill, A., Yoden, S., Charlton, A. J., Hio, Y., Lahoz, W. A., and Mori, A.: Major stratospheric warming in the southern hemisphere in 2002: dynamical aspects of the ozonehole split, SPARC Newsletter, 20, 24–26, 2003.

Chanin, M. L. and Hauchecorne, A.: Lidar studies of temperature and density using Rayleigh scattering, in: Handbook for MAP: Ground-Based Techniques, edited by: Vincent, R. A., 13, 7, Scientific Committee on Solar Terrestrial Physics, International Council of Scientific Unions, Urbana, IL. 1984.

Delisi, D. P. and Dunkerton, T. J.: Seasonal variation of the semiannual oscillation, J. Atmos. Sci., 45, 2772–2787, 1988.

Donfrancesco, G., Adriani, A., Gobbi, G. P., and Congeduti, F.: Lidar observations of stratospheric temperatures above McMurdo Station (78 S, 167 E), Antarctica , J. Atmos. Terr. Phys., 58, 1391–1399, 1996.

Duck, T. J., Whiteway, J. A., and Carswell, A. I.: Lidar observations of gravity wave activity and Arctic stratospheric vortex core warming, Geophys. Res. Lett., 25, 2813–2816, 1998.

Dunkerton, T. J. and Delisi, D. P.: Evolution of potential vorticity in the winter stratosphere of January–February 1979, J. Geophys. Res., 91, 1199–1208, 1986.

Dunkerton, T. J., Delisi, D. P., and Baldwin, M. P.: Distribution of major stratospheric warmings in relation to the quasi-biennial oscillation, Geophys. Res. Lett., 15, 136–139, 1988.

Dunkerton, T. J. and Baldwin, M. P.: Quasi-biennial Modulation of Planetary-Wave Fluxes in the Northern Hemisphere Winter, J. Atmos. Sci., 48, 1043–1061, 1991.

Hansen, J., Russell, G., Rind, D., Stone, P., Lacis, A., Lebedeff, S., Ruedy, R., and Travis, L.: Efficient three-dimensional global models for climate studies: Models I and II, Mon. Weather Rev., 111, 609–662, 1983.

Hauchecorne, A. and Chanin, M. L.: Density and temperature profiles obtained by lidar between 35 and 70 km, Geophys. Res. Lett., 8, 565–568, 1980.

Hauchecorne, A. and Chanin, M. L.: Mid latitude observations of planetary waves in the middle atmosphere during the winter over 1981–1982, J. Geophys. Res., 88, 3843–3849, 1983.

Hauchecorne, A., Chanin, M. L., and Keckhut, P.: Climatology and trends of the middle atmospheric temperature (33–87 KM) as seen by Rayleigh LiDAR over the South of France, J. Geophys. Res., 96(D8), 15 297–15 309, 1991.

Hauchecorne, A., Godin, S., Marchand, M., Heese, B., and Souprayen, C.: Quantification of the transport of chemical constituents from the polar vortex to midlatitudes in the lower stratosphere using the high-resolution advection model MIMOSA and effective diffusivity, J.

Geophys. Res., 107(D20), 8289, doi:10.1029/2001JD000491, 2002.
Heese, B., Godin, S., and Hauchecorne, A.: Forecast and simulation of stratospheric ozone filaments: A validation of a high-resolution PV advection model by airborne ozone lidar measurements in winter 1998–1999, J. Geophys. Res., 106(D17), 20 011–20 024, 2001.
Hervig, M. E., Russell III, M., Gordley, L. L., Drayson, S. R., Stone, K., Thompson, E., Gelman, M. E., and McDermid, I. S.: A validation of temperature measurements from the Halogen occultation Experiment, J. Geophys. Res., 101(D6), 10 277–10 286, 1996.
Holton, J. R., Pyle, J. A., and Curry, J. A.: Encyclopedia of Atmospheric Sciences, Elsevier, 1342–1353, 2002.
Holton, J. R. and Austin, J.: The influence of the QBO on sudden stratospheric warmings, J. Atmos. Sci., 48, 607–618, 1991.
Jacobi, C., Kurschner, D., Müller, H. G., Pancheva, D., Mitchell, N. J., and Naujokat, B.: Response of the mesopause region dynamics to the February 2001 stratospheric warming, J. Atmos. Terr. Phys., 65, 843–855, 2003.
Kalnay, E., Kanamitsu, M., Kistler, R., Collins, W., Deaven, D., Gandin, L., Iredell, M., Saha, S., White, G., Woollen, J., Zhu, Y., Chelliah, M., Ebisuzaki, W., Higgins, W., Janowiak, J., Mo, K., Ropelewski, C., Wang, J., Leetmaa, A., Reynolds, R., Jenne, R., and Joseph, D.: The NCEP/ NCAR 40-year re-analysis project, B. Am. Meteorol. Soc., 77, 437–471, 1996.
Kanzawa, H.: Four observed sudden stratospheric warmings diagnosed by the Eliassen-Palm flux and refractive index, Dynamics of the Middle Atmosphere, in: Proceedings of a U.S.-Japan Seminar, Honolulu, Hawaii, 8–12 November, 1982, edited by: Holton, J. R. and Matsuno, T., 307–331, 1984.
Labitzke, K.: Inter-annual variability of the winter stratosphere in the northern hemisphere, Mon. Weather Rev., 105, 762–770, 1977.
Labitzke, K.: Stratospheric-mesospheric midwinter disturbances: a summary of observed characteristics, J. Geophys. Res., 86, 9665–9678, 1981.
Labitzke, K.: The amplification of height wave 1 in January 1979: A characteristic precondition for the major warming in February, Mon. Weather Rev., 109, 983–989, 1981.
Labitzke, K., Lenschow, R., Naujokat, B., and Petzoldt, K.: First information on the major mid-winter warming in February 1981, Beilage zur Berliner Wetterkarte, SO 4/81, 1981.
Labitzke, K.: On the interannual variability of the middle stratosphere during the northern winters, J. Meteorol. Soc. Jpn., 60, 124–139, 1982.
Labitzke, K.: Sunspots, the QBO, and the stratospheric temperature in the north polar region,

Geophys. Res. Lett., 14, 535–537, 1987.
Labitzke, K. and van Loon, H.: The Stratosphere-Phenomena, History, and Relevance, Springer, Berlin, 1999.
Labitzke, K. and Kunze, M.: Stratospheric temperatures over the Arctic: Comparison of three data sets, Meteorolog. Z., 14, 65–74, 2005.
Leblanc, T., McDermid, I. S., She, C. Y., Krueger, D. A., Hauchecorne, A., and Keckhut, P.: Temperature climatology of the middle atmosphere from long-term lidar measurements at mid- and low-latitudes, J. Geophys. Res., 103, 17 191–17 204, 1998.
Limpasuvan, V., Thompson., D. W. J., and Hartmann, D. L. : The life cycle of Northern Hemisphere sudden stratospheric warmings, J. Climate, 17, 2584–2596, 2004.
Lorenz, E. N.: The nature and theory of general circulation of the atmosphere, No. 218, 161 pp., World Meteorological Organization, Geneva, 1967.
Manney, G. L., Kruger, K., Sabutis, J. L., Sena, S. A., and Pawson, S.: The remarkable 2003–2004 winter and other recent warm winters in the Artic stratosphere since the late 1990s, J. Geophys. Res., 100, doi:10.1029/2004JD006367, 2005.
Manney, G. L., Lahoz, W. A., Swinbank, R., O'Neill, A., Connew, P. M., and Zurek, R. W.: Simulation of the December 1998 stratospheric major warming, Geophys. Res. Lett., 26, 2733–2736, 1999.
Marchand, M., Godin, S., Hauchecorne, A., Lefévre, F., Bekki, S., and Chipperfield, M.: Influence of polar ozone loss on northern mid-latitude regions estimated by a high-resolution chemistry transport model during winter 1999/2000, J. Geophys. Res., 108(D5), 8326, doi:10.1029/2001JD000906, 2003.
Marenco, F., Santacesaria, V., Bais, A., Balis, D., di Sarra, A., Papayannis, A., and Zerefos, C. S.: Optical properties of tropospheric aerosols determined by lidar and spectrophotometric measurements (PAUR campaign), Appl. Opt., 36, 6875–6886, 1997.
Matsuno, T.: A dynamical model of the stratospheric sudden warming, J. Atmos. Sci., 28, 1479–1494, 1971.
McIntyre, M. E.: How well do we understand the dynamics of stratospheric warmings?, J. Meteorol. Soc. Jpn., 60, 37–65, 1982.
McIntyre, M. E. and Palmer, T. N.: Breaking planetary waves in the stratosphere, Nature, 305, 593–600, 1983.
Mechoso, C. R., Hartmann, D. L., and Farrara, J. D.: Climatology and interannual variability of wave, mean-flow interaction in the Southern Hemisphere, J. Atmos. Sci., 42, 2189–2206,

1985.
Morel, B., Bencherif, H., Keckhut, P., Portafaix, T., Hauchecorne, A., and Baldy, S.: Fine-scale study of a thick stratospheric ozone lamina at the edge of the southern subtropical barrier: 2. Numerical simulations with coupled dynamics models, J. Geophys. Res., 110, D17101, doi:10.1029/2004JD005737, 2005.
Naujokat, B.: An update of the observed quasi-biennial oscillation of the stratospheric winds over the tropics, J. Atmos. Sci., 43, 1873–1877, 1986.
Naujokat, B. and Labitzke, K.: Collection of reports on the stratospheric circulation during the winters 1974/75–1991/92, STEP Handbook, July 1993, SCOSTEP Urbana, Illinois, USA, 1993.
Naujokat, B., Krüger, K., Matthes, K., Hoffmann, J., Kunze, M., and Labitzke, K.: The early major warming in December 2001 – exceptional?, Geophys. Res. Lett., 29, doi:10.1029/2002GL015316, 2002.
Nee, J. B., Thulasiraman, S., Chen, W. N., VenkatRatnam, M., and Narayana Rao, D.: Middle atmospheric temperature structure over two tropical locationas, Chung Li (25° N,121° E) and Gadanki (13.5° N,79.2° E), J. Atmos. Sol.-Terr. Phy., 64, 1311–1319, 2002.
O'Neill, A. and Taylor, B. F.: Study of the major stratospheric warming of 1976–77, Quart. J. Roy. Meteor. Soc., 105, 75–92, 1979.
O'Neill, A.: Stratospheric Sudden Warmings, Encyclopedia of Atmospheric Sciences, 1342–1353, 2003.
Quiroz, R. S., Miller, A. J., and Nagatani, R. M.: A comparison of observed and simulated properties of sudden stratospheric warmings, J. Atmos. Sci., 32, 1723–1736, 1975.
Quiroz, R. S.: The tropospheric-stratospheric polar vortex breakdown of January 1977, Geophys. Res. Lett., 4, 151–154, 1977.
Quiroz, R. S.: The association of stratospheric warmings with tropospheric blocking, J. Geophys. Res., 91, 5277–5285, 1986.
Randel, W. J. and Boville, B. A.: Observations of Major Stratospheric Warming during December 1964, J. Atmos. Sci., 44, 2179–2186, 1987.
Randel, W., Fleming, E., Geller, M., Gelman, M., Hamilton, K., Karoly, D., Ortland, D., Pawson, S., Swinbank, R., Udelhofen, P., Wu, F., Baldwin, M., Chanin, M.-L., Keckhut, P., Labitzke, K., Remsberg, E., Simmons, A., and Wu, D.: The SPARC Intercomparison of Middle Atmosphere Climatologies, WCRP – 116, WMO/TD-No. 1142, SPARC Report No. 3, December, 2002.

Roble, R. G. and Dickinson, R. E.: How will changes in carbon dioxide and methane modify the mean structure of the mesosphere and thermosphere?, Geophys. Res. Lett., 16, 1441–1444, 1989.
Scherhag, R.: Die explosionsartigen Stratosphärenerwärmungen des Spätwinters 1951/52. Berichte des deutschen Wetterdienstes in der US-Zone, 6, 38, 51–63, 1952.
Schoeberl, M. R.: Stratospheric warmings: Observations and theory, Rev. Geophys. Space. Phys., 16, 521–538, 1978.
Sivakumar, V., Rao, P. B., and Krishnaiah, M.: Lidar studies of Stratosphere-Mesosphere Thermal Structure over Low Latitude: Comparison with satellite and models, J. Geophys. Res., 108(D11), 4342, doi:10.1029/2002JD003029, 2003.
Sivakumar, V., Morel, B., Bencherif, H., Baray, J. L., Baldy, S., Hauchecorne, A., and Rao, P. B.: Rayleigh lidar observation of a warm stratopause over a tropical site, Gadanki (13.5° N; 79.2° E), Atmos. Chem. Phys., 4, 1989–1996, 2004, http://www.atmos-chem-phys.net/4/1989/2004/.
Sivakumar, V., Bencherif, H., Hauchecorne, A., Keckhut, P., Narayana Rao, D., Sharma, S., Chandra, H., Jayaraman, A., and Rao, P. B.: Rayleigh lidar observations of double stratopause structure over three different northern hemisphere stations, Atmos. Chem. Phys. Discuss., 6, 6933–6956, 2006, http://www.atmos-chem-phys-discuss.net/6/6933/2006/.
Walterscheid, R. L., Sivjee, G., and Roble, R. G.: Mesospheric and lower thermospheric manifestations of a stratospheric warming event over Eureka, Canada (80° N), Geophys. Res. Lett., 27, 2897–2900, 2000.
Whiteway, J. A. and Carswell, A. I.: Rayleigh Lidar Observations of Thermal Structure and Gravity Wave Activity in the High Arctic during a Stratospheric Warming, J. Atmos. Sci., 51, 3122–3136, 1994.
Whiteway, J. A., Duck, T. J., Donovan, D. P., Bird, J. C., Pal., S. R., and Carswell, A. I.: Measurements of gravity wave activity within and around the Arctic stratospheric vortex, Geophys. Res. Lett., 24, 1387–1390, 1997.

Table 1. Statistics of SSW events observed over OHP.

Date of SSW observed		ΔT	Height (km)			Reference
NCEP	OHP	(K)	SSW	S_w	S_d	
4 to 6 Dec 1981	2 Jan 1982 $^{-,m}$	11.0	50	50	0	Hauchecorne and Chanin (1983)
	31 March 1982 $^{+,M}$	18.1	54	50	−4	Naujokat and Labitzke (1993)
17 Dec 1982	22 Dec 1982 $^{+,M}$	15.2	45	47	2	-do-
	28 Dec 1982 $^{+,m}$	19.4	46	47	1	
	21 Jan 1983 $^{+,m}$	14.6	48	47	−1	-do-
	28 Jan 1983 $^{+,m}$	17.9	47	47	0	
	09 Nov 1983 $^{-,m}$	12.7	47	47	0	Naujokat and Labitzke (1993)
24 to 27 Feb 1984	23 Feb 1984 $^{-,M}$	15.8	46	47	1	
01 to 31 March 1984	04 March 1984 $^{-,M}$	14.5	45	47	2	
	4 Dec 1984 $^{+,m}$	10.2	44	44	0	Randel and Boville (1987)
	11 Dec 1984 $^{+,m}$	13.0	43	44	1	-do-
1 to 5 Jan 1985	1 Jan 1985 $^{+,M}$	22.0	38	44	6	
	14 March 1985 $^{+,m}$	11.7	42	44	2	
	27 Nov 1985 $^{-,m}$	17.3	50	49	−1	
	1 Dec 1986 $^{-,m}$	14.1	47	47	0	Manney et al. (2005)
	23 Dec 1986 $^{-,m}$	19.2	48	47	−1	
	4 Jan 1987 $^{-,m}$	17.7	42	47	5	
23 to 27 Jan 1987	23 Jan 1987 $^{-,M}$	35.7	43	47	4	
21 to 24 Feb 1987	27 Feb 1987 $^{-,M}$	12.2	41	47	6	
	24 March 1987 $^{-,m}$	11.0	48	47	−1	
	21 Feb 1988 $^{-,m}$	18.7	54	49	−5	Baldwin and Dunkerton (1989)
	17 Dec 1988 $^{-,m}$	32.8	46	49	3	
	5 Jan 1989 $^{-,m}$	19.3	46	49	3	
	5 Jan 1990 $^{+,m}$	21.8	46	47	1	Hauchecorne at al. (1991)
	9 Feb 1990 $^{+,m}$	17.2	46	47	1	
	5 Dec 1991 $^{-,m}$	11.1	49	48	−1	
	15 Dec 1991 $^{+/-,m}$	27.0	43	48	5	
	15 Jan 1992 $^{+,m}$	16.6	47	48	1	
	12 March 1992 $^{+,m}$	10.3	47	48	1	
	7 Feb 1994 $^{-,m}$	20.0	49	48	−1	
	13 Jan 1995 $^{+,m}$	28.8	44	48	4	
	18 Dec 1995 $^{-,m}$	24.0	48	49	1	
	15 Feb 1996 $^{-,m}$	21.3	43	49	6	
	3 Dec 1997 $^{-,m}$	32.2	54	48	−6	
	6 Dec 1998 $^{+,m}$	15.1	46	46	0	Manney et al. (1999)
15 to 21 Dec 1998	17 Dec 1998 $^{+,M}$	28.7	40	46	6	
	7 Jan 1999 $^{+,m}$	18.1	44	46	2	
	14 Jan 1999 $^{+,m}$	14.4	43	46	3	
	22 Dec 1999 $^{-,m}$	17.9	45	48	3	
	30 Dec 1999 $^{-,m}$	26.5	45	48	3	
	4 Feb 2000 $^{-,m}$	17.3	47	48	1	
21, 22 March 2000	27 March 2000 $^{-,M}$	19.1	44	48	4	
12 to 23 Feb 2001	15 Feb 2001 $^{+/-,M}$	15.6	44	47	3	Jacobi et al. (2003)

Where, +/− stands for QBO phase west/east; M – Major warming (10), m – minor warming (33), S_w and S_d indicates the winter stratopause and descent of stratopause height.

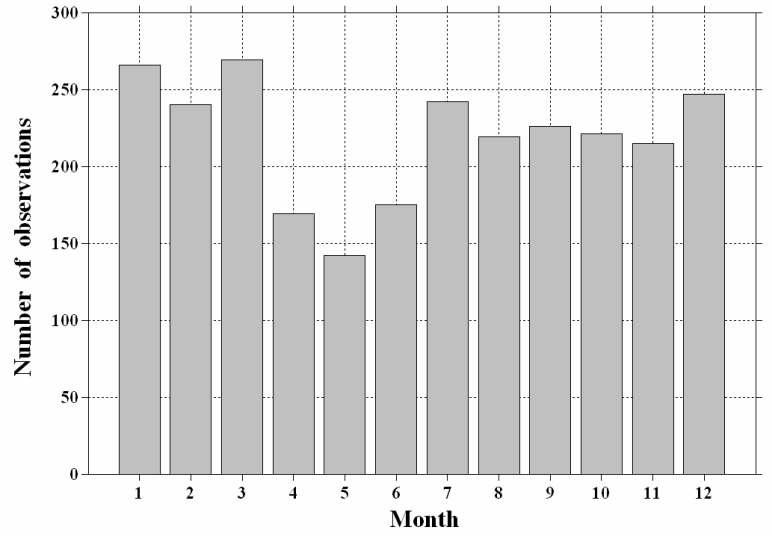

Fig. 1. Monthly distribution of number of OHP lidar observations used from 1 January 1982 to 6 November 2001.

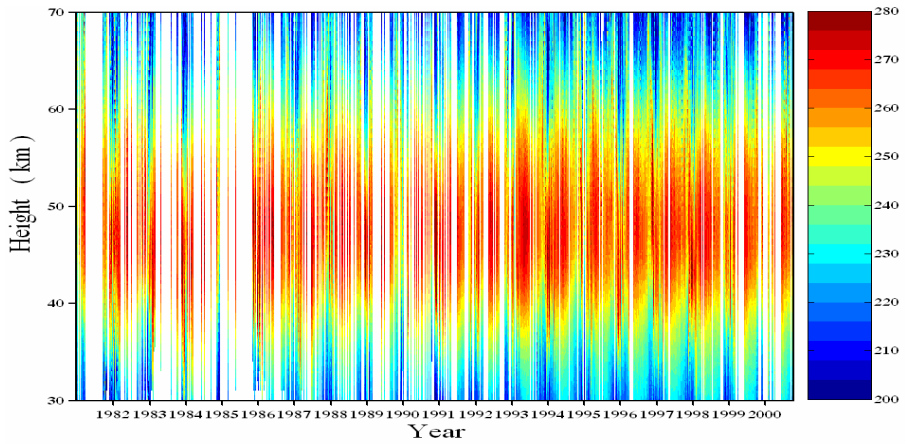

Fig. 2. Temporal evolution of temperature observed from 1 January 1982 to 6 November 2001, the blank space in the figure indicates actual data gap.

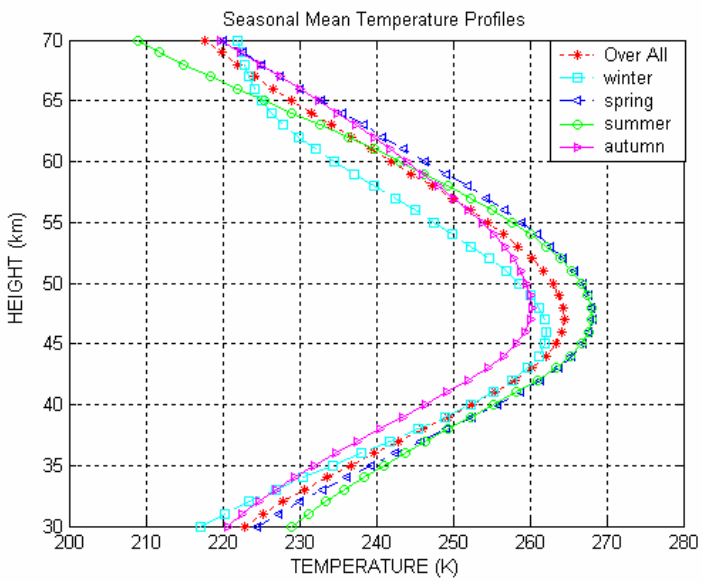

Fig. 3. Seasonal mean temperature profiles obtained from the data during the year 1982 to 2001.

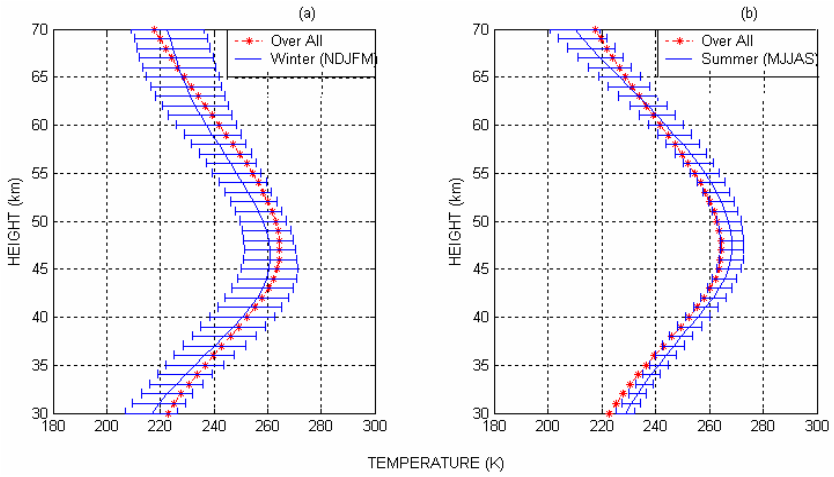

Fig. 4. Over-all mean and seasonal temperature profile during **(a)** winter and **(b)** summer along with the standard deviations obtained from the data during the year 1982 to 2001. The standard deviation is shown for the seasonal temperature profile.

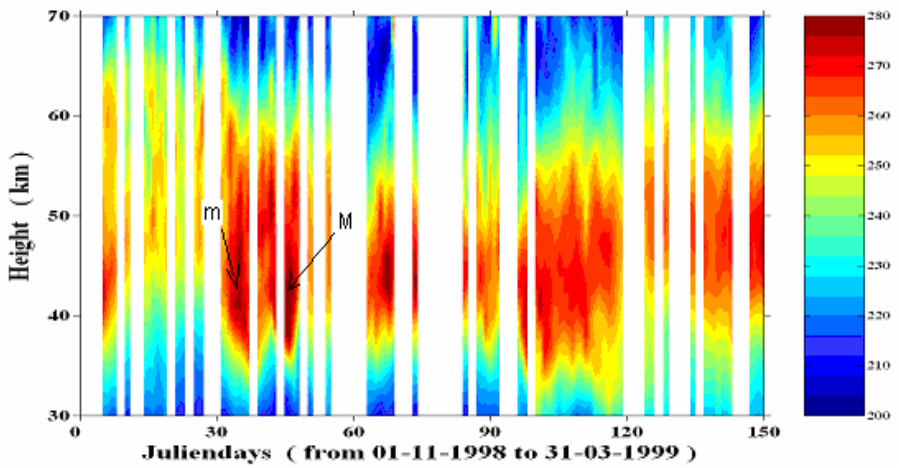

Fig. 5. Time evolution of OHP temperature starting from 1 November 1998 to 31 March 1999, "m" – minor SSW (6 December 1998), "M" – major SSW (17 December 1998).

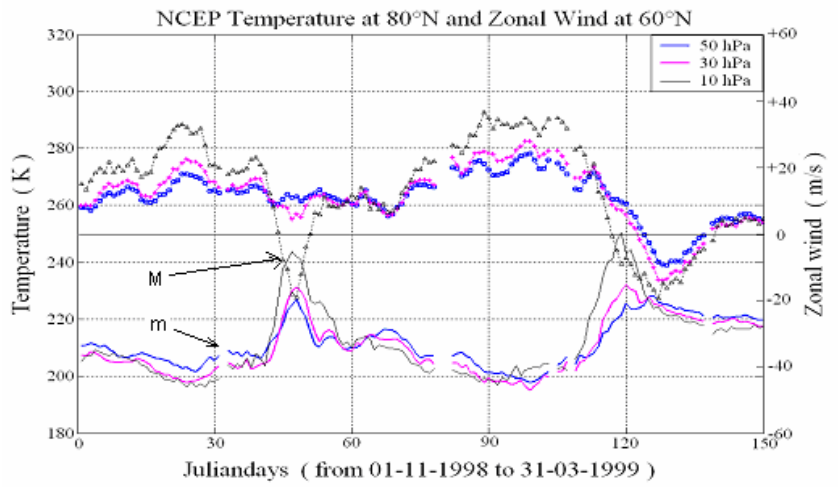

Fig. 6. Time evolution of NCEP data of zonal-mean temperature at 80° N and zonal mean wind at 60° N at 50, 30 and 10 hPa level during 1 November 1998 to 31 March 1999. The solid line denotes temperature and the line with legend denotes wind. "m" – minor SSW (6 December 1998), "M" – major SSW (17 December 1998).

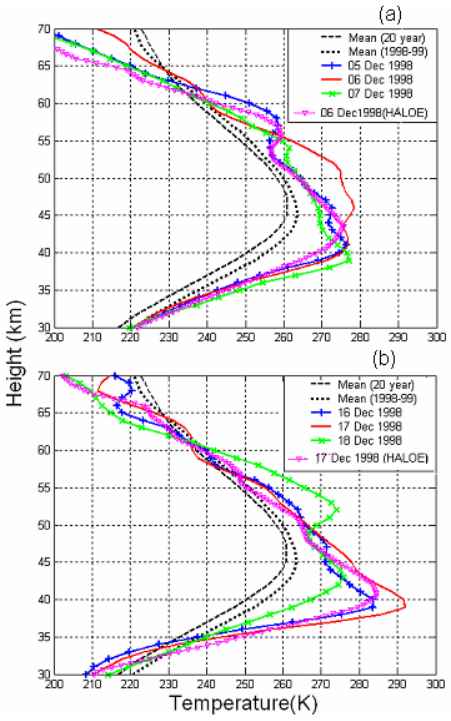

Fig. 7. Height profile of temperature for the first **(a)** and the second **(b)** warming occasions observed during 4–8 December 1998 and 16–19 December 1998. The overall and yearly mean profiles are superimposed in the same figure (see, Legend). The HALOE temperature measurements corresponds to the same day and overpass near to OHP lidar station.

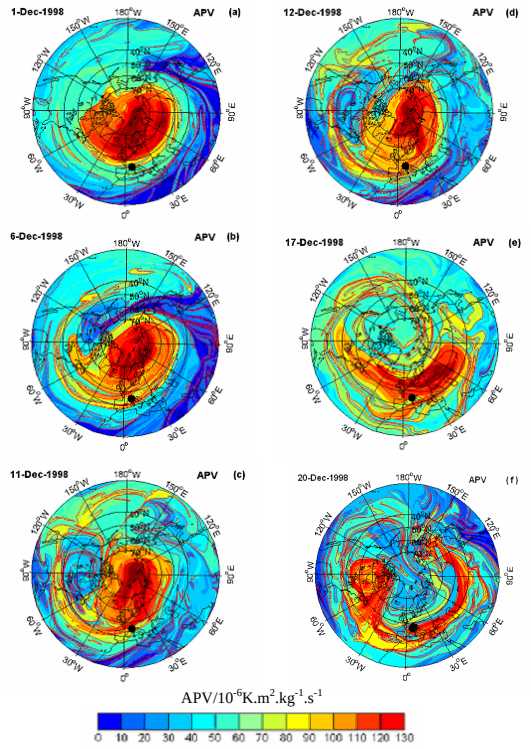

Fig. 8. North Polar stereographic maps of advected PV (APV) at 950 K provided by MIMOSA simulation driven by the ECMWF ERA40 reanalysis data for the selected days in December 1998. The outermost circle designates the Equator, and "•" indicates the location of OHP lidar site (44° N, 6° E).

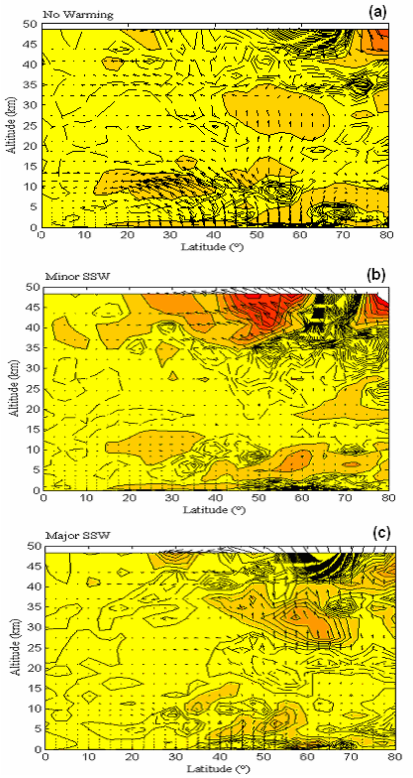

Fig. 9. Meridional cross section of Eliassen-Palm Flux and Zonal mean wind velocity. Contours represent div (F), in m.s-1 per day; Regions of easterly winds (negative values) are shaded **(a)** no warming (normal winter situation) **(b)** minor SSW on 6 December 1998 **(c)** major SSW 17 December 1998.

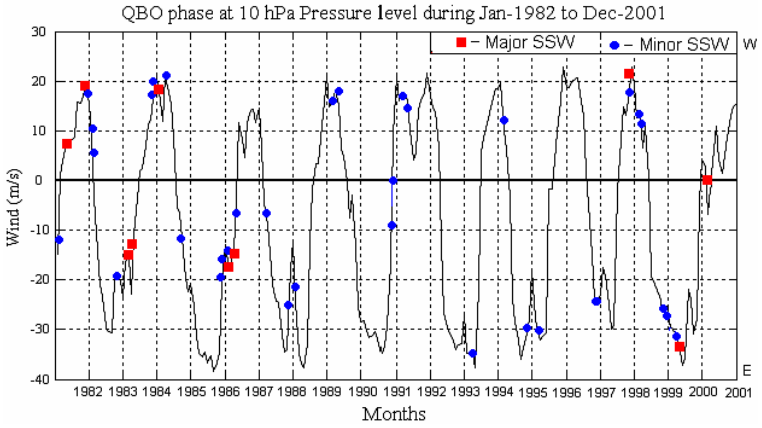

Fig. 10. QBO signature in monthly mean zonal wind obtained from a near equatorial region (Singapore; 1.30° N. 103.85° E); occurrence of major (red square marks) and minor (blue dots) warmings for the period from the year 1981 to 2001.